

1 Dilution impacts on smoke aging: Evidence in BBOP data

2

3 Anna L. Hodshire¹, Emily Ramnarine¹, Ali Akherati², Matthew L. Alvarado³, Delphine K. Farmer⁴,
4 Shantanu H. Jathar², Sonia M. Kreidenweis¹, Chantelle R. Lonsdale³, Timothy B. Onasch⁵, Stephen R.
5 Springston⁶, Jian Wang^{6,a}, Yang Wang^{7,b}, Lawrence I. Kleinman⁶, Arthur J. Sedlacek III⁶, Jeffrey R.
6 Pierce¹

7 ¹Department of Atmospheric Science, Colorado State University, Fort Collins, CO 80523, United States

8 ²Department of Mechanical Engineering, Colorado State University, Fort Collins, CO 80523, United States

9 ³Atmospheric and Environmental Research, Inc., Lexington, MA 02421, United States

10 ⁴Department of Chemistry, Colorado State University, Fort Collins, CO 80523, United States

11 ⁵Aerodyne Research Inc., Billerica, MA 01821, United States

12 ⁶Environmental and Climate Sciences Department, Brookhaven National Laboratory, Upton, NY 11973, United States

13 ⁷Center for Aerosol Science and Engineering, Washington University, St. Louis, MO 63130, United States

14 ^aNow at Center for Aerosol Science and Engineering, Washington University, St. Louis, MO 63130, United States

15 ^bNow at Department of Civil, Architectural and Environmental Engineering, Missouri University of Science and Technology,
16 Rolla, Missouri 65409, United States

17

18

19

20

21

22

23

24

25

26

27 *Correspondence to:* Anna L. Hodshire (Anna.Hodshire@colostate.edu)

28 **Abstract.** Biomass burning emits vapors and aerosols into the atmosphere that can rapidly evolve as smoke plumes travel
29 downwind and dilute, affecting climate- and health-relevant properties of the smoke. To date, theory has been unable to
30 explain **observed** variability in smoke evolution. Here, we use observational data from the BBOP field campaign and show
31 that initial smoke organic aerosol mass concentrations can help predict changes in smoke aerosol aging markers, number
32 concentration, and **number-**mean diameter between 40-262 nm. Because initial field measurements of plumes are generally
33 >10 minutes downwind, smaller plumes will have already undergone substantial dilution relative to larger plumes **and have**
34 **lower concentrations of smoke species at these observations closest to the fire. However,** the extent to which dilution has
35 occurred prior to the first observation is not a directly measurable quantity. Hence, initial observed plume concentrations can
36 serve as a rough indicator of the extent of dilution prior to the first measurement, which impacts photochemistry, **and** aerosol
37 evaporation, **and coagulation**. Cores of plumes have higher concentrations than edges. By segregating the observed plumes
38 into cores and edges, we **find evidence** ~~infer~~ that particle aging, evaporation, and coagulation occurred before the first
39 measurement. We further find that on the **plume** edges, the ~~oxidation state of~~ organic aerosol **is more oxygenated** ~~has~~

40 increased while a marker for primary biomass burning aerosol emissions has decreased in relative abundance than in the
41 plume cores. and undergone more decreases in a marker for primary biomass burning organic aerosol. Finally, we attempt to
42 decouple the roles of the initial concentrations and time since emission by ~~but~~ performing multivariate linear regression of
43 various aerosol properties (composition, size) on these two factors.

44 1 Introduction

45 Smoke from biomass burning is a major source of atmospheric primary aerosol and vapors (Akagi et al., 2011;
46 Gilman et al., 2015; Hatch et al., 2015, 2017; Jen et al., 2019; Koss et al., 2018; Reid et al., 2005; Yokelson et al., 2009),
47 influencing air quality, local radiation budgets, cloud properties, and climate (Carrico et al., 2008; O'Dell et al., 2019; Petters
48 et al., 2009; Ramnarine et al., 2019; Shrivastava et al., 2017), as well as the health of ~~smoke~~-impacted communities (Ford et
49 al., 2018; Gan et al., 2017; Reid et al., 2016). Dilution of a smoke plume occurs as the plume travels downwind, mixing with
50 regional 'background' air, reducing the concentrations of the smoke aerosols and vapors and ~~potentially driving~~ allowing for
51 ~~rapid~~ changes in the physical and chemical properties of the emissions. ~~Dilution of a smoke plume occurs when the plume~~
52 ~~mixes with regional 'background' air, reducing the concentrations of the smoke aerosols and vapors as the plume travels~~
53 ~~downwind. Dilution can lead to rapid changes in the physical and chemical properties of the emissions. Dilution through~~
54 ~~entrainment of regional background air can cause vapors and particles emitted from fires to rapidly evolve as smoke travels~~
55 ~~downwind~~ (Adachi et al., 2019; Akagi et al., 2012; Bian et al., 2017; Cubison et al., 2011; Hecobian et al., 2011; Hodshire et
56 al., 2019a, 2019b; Jolleys et al., 2012, 2015; Konovalov et al., 2019; May et al., 2015; Noyes et al., 2020; Sakamoto et al.,
57 2015, Palm et al., 2020). Fires span an immense range in size, from small agricultural burns, which may be only a few m² in
58 total area and last a few hours, to massive wildfires, which may burn 10,000s of km² over the course of weeks (Andela et al.,
59 2019). This range in size leads to variability in initial plume size and extent of dilution by the time of the first measurement. ~~¶~~
60 ~~as~~ Large, thick plumes dilute more slowly than small, thin plumes for similar atmospheric conditions, ~~as the cores of larger~~
61 ~~plumes are at a greater physical distance to the background air, shielding them from dilution for longer~~ (Akagi et al., 2012;
62 Bian et al., 2017; Cubison et al., 2011; Hecobian et al., 2011; Hodshire et al., 2019a, 2019b; Jolleys et al., 2012, 2015;
63 Konovalov et al., 2019; May et al., 2015; Sakamoto et al., 2015, Lee et al., 2020, Garofalo et al., 2019). Plumes can dilute
64 unevenly, with edges of the plume mixing in with surrounding air more rapidly than the core of the plume. Variability in
65 dilution leads to variability in the evolution of smoke emissions as instantaneous plume aerosol concentrations will control
66 shortwave radiative fluxes (and thus photolysis rates and oxidant concentrations), gas-particle partitioning, and particle
67 coagulation rates (Akagi et al., 2012; Bian et al., 2017; Cubison et al., 2011; Hecobian et al., 2011; Hodshire et al., 2019a,
68 2019b; Jolleys et al., 2012, 2015; Konovalov et al., 2019; May et al., 2015; Sakamoto et al., 2015, Garofalo et al., 2019,
69 Ramnarine et al., 2019; Sakamoto et al., 2016). Thus, capturing variability in plume aerosol concentrations and dilution
70 between fires and within fires can aid in understanding how species change within the first few hours of emission for a range
71 of plume sizes.

72 The evolution of total particulate matter (PM) or organic aerosol (OA) mass from smoke has been the focus of
73 many studies, as PM influences both human health and climate. Secondary organic aerosol (SOA) production ~~occurs~~
74 ~~come about~~ through oxidation of gas-phase volatile organic compounds (VOCs) that can form lower-volatility products that
75 partition to the condensed phase (Jimenez et al., 2009; Kroll and Seinfeld, 2008). SOA formation may also arise from
76 heterogeneous and multi-phase reactions in both the organic and aqueous phases (Jimenez et al., 2009; Volkamer et al.,
77 2009). In turn, oxidant concentrations depend on shortwave fluxes (Tang et al., 1998; Tie, 2003; Yang et al., 2009) and the
78 composition of the plume (Yokelson et al. 2009; Akagi et al. 2012; Hobbs et al. 2003; Alvarado et al. 2015). Smoke particles
79 contain semivolatile organic compounds (SVOCs) (Eatough et al., 2003; May et al., 2013), which may evaporate off of
80 particles as the plume becomes more dilute (Huffman et al. 2009; May et al. 2013; Garofalo et al. 2019; Grieshop et al.
81 2009), leading to losses in total aerosol mass. Field observations of smoke PM and OA mass normalized for dilution (e.g.
82 through an inert tracer such as CO) report that for near-field (<24 hours) physical aging, net PM or OA mass can increase
83 (Cachier et al., 1995; Formenti et al., 2003; Liu et al., 2016; Nance et al., 1993; Reid et al., 1998; Vakkari et al., 2014, 2018;
84 Yokelson et al., 2009), decrease (Akagi et al., 2012; Hobbs et al., 2003; Jolleys et al., 2012, 2015; May et al., 2015), or
85 remain nearly constant (Brito et al., 2014; Capes et al., 2008; Collier et al., 2016; Cubison et al., 2011; Forrister et al., 2015;
86 Garofalo et al., 2019; Hecobian et al., 2011; Liu et al., 2016; May et al., 2015; Morgan et al., 2019; Sakamoto et al., 2015;
87 Sedlacek et al., 2018; Zhou et al., 2017). It is theorized that both losses and gains in OA mass are likely happening
88 concurrently in most plumes through condensation and evaporation (May et al. 2015; Hodshire et al. 2019; Hodshire et al.
89 2019; Bian et al. 2017; Palm et al. 2020)(~~Bian et al., 2017; Hodshire et al., 2019a, 2019b; May et al., 2015~~), with the balance
90 between the two determining whether net increases or decreases or no change in mass occurs during near-field aging.
91 However, there is currently no reliable predictor of how smoke aerosol mass (normalized for dilution) may change for a
92 given fire.

93 Evolution of total aerosol number, size, and composition is critical for improving quantitative understanding of how
94 biomass burn smoke plumes impact climate. These impacts include smoke aerosols' abilities to both act as cloud
95 condensation nuclei (CCN) and to scatter/absorb solar radiation, each of which is determined by particle size and
96 composition (Albrecht, 1989; Petters and Kreidenweis, 2007; Seinfeld and Pandis, 2006; Twomey, 1974; Wang et al., 2008).
97 Particles can increase or decrease in size as well as undergo compositional changes through condensation or evaporation of
98 ~~more volatile compounds~~vapors. In contrast, coagulation always decreases total number concentrations and increases
99 average particle diameter. Plumes with higher aerosol number concentrations will undergo more coagulation than those
100 with lower concentrations (Sakamoto et al., 2016).

101 Being able to predict smoke aerosol mass, number, size, and composition accurately is an essential component in
102 constraining the influence of fires on climate, air quality, and health. Fires in the western United States region are predicted
103 to increase in size, intensity, and frequency (Dennison et al., 2014; Ford et al., 2018; Spracklen et al., 2009; Yue et al., 2013).
104 In response, several large field campaigns have taken place in the last 7 years examining wildfires in this region (Kleinman
105 et al., 2020~~Kleinman and Sedlacek 2016~~; Garofalo et al. 2019; Palm et al., 2020). Here, we present smoke plume

106 observations from the Biomass Burning Observation Project (BBOP) campaign of aerosol properties from five research
107 flights sampling wildfires downwind in seven pseudo-Lagrangian sets of transects to investigate the evolution of OA mass
108 and oxidation state, aerosol number, and aerosol ~~number~~ mean diameter. A range of initial (at the time of the first plume pass
109 in the aircraft) plume OA mass concentrations were captured within these flights and ~~sufficiently~~ fast (1 second)
110 measurements of aerosols and key vapors were taken. ~~The time resolution of the data was great enough that we have been~~
111 ~~able to~~ We segregate each transect into edge, core, or intermediate regions of the plume and examine aerosol properties
112 within the context of both the location within the plume (edge, core, or intermediate) and the initial OA mass loading of the
113 given location. The differences in aerosol loading serve as a proxy for differences in ~~initial fire and plume sizes, mass fluxes,~~
114 ~~and subsequent amount of dilution. rates, as t~~ The extent to which dilution has occurred prior to the first observation is not a
115 measurable quantity, ~~and fire sizes and mass fluxes were not estimated as a part of the BBOP campaign.~~ We create
116 mathematical fits for predicting OA oxidation markers and mean particle diameter given initial plume OA mass
117 ~~concentration~~ and physical age (time) of the smoke. These fits may be used to evaluate other smoke datasets and assist in
118 building parameterizations for regional and global climate models to better-predict smoke aerosol climate and health
119 impacts.

120 **2 Methods**

121 The BBOP field campaign occurred in 2013 and included a deployment of the United States Department of Energy
122 Gulfstream 1 (G-1) research aircraft in the Pacific Northwest region of the United States (Kleinman and Sedlacek, 2016;
123 Sedlacek et al., 2018) from June 15 to September 13. We analyze five cloud-free BBOP research flights that had seven total
124 sets of across-plume transects that followed the smoke plume downwind in a Lagrangian manner (see Figs. S1-S6 for
125 examples; Table S1) from approximately 15 minutes after emission to 2-4 hours downwind (Kleinman and Sedlacek, 2016).
126 The G-1 sampling setup is described in (Kleinman and Sedlacek, 2016; Sedlacek et al., 2018; Kleinman et al., 2020).

127 Number size distributions were obtained with a Fast-integrating Mobility Spectrometer (FIMS), providing particle
128 size distributions nominally from approximately 20-350 nm (Kulkarni and Wang, 2006; Olfert and Wang, 2009); data was
129 available between 20-262 nm for the flights used in this study. A Soot Photometer Aerosol Mass Spectrometer (SP-AMS)
130 provided organic and inorganic (sulfate, chlorine, nitrate, ammonium) ~~aerosol mass concentration of PM₁ (sub-micron~~
131 ~~aerosol) PM₁ aerosol masses~~ (Canagaratna et al. 2007), select fractional components (the fraction of the AMS OA spectra at
132 a given mass-to-charge ratio) (Onasch et al., 2012), and elemental analysis (O/C and H/C) (Aiken et al., 2008; Canagaratna
133 et al., 2015). ~~Extended details on the SP-AMS are provided in Text S1 in the supplementary information, and but a briefer~~
134 ~~overview is given here.~~ The SP-AMS had ~~its~~ the highest sensitivity between 70-500 nm, dropping to 50% of peak
135 ~~sensitivity~~ ~~transmission efficiency~~ by 1000 nm (Liu et al. 2007). It was characterized to have a collection efficiency of 0.5
136 when the instrument's laser was off and 0.76 when the instrument's laser was on during the BBOP campaign, and these
137 corrections have been applied to the data. ~~There is substantial evidence from other studies that the in the published literature~~

138 for the CE of the tungsten vaporizer (laser off mode) (Lim et al., 2019) and the laser vaporizer (laser on mode) (Willis et al.,
139 2014) to change as a function of chemical composition, rBC coating thickness, size, and sphericity in laboratory studies
140 (Middlebrook et al., 2012; Willis et al., 2014; Corbin et al., 2015; Massoli et al., 2015; Collier et al., 2018) and in aircraft
141 observations (Kleinman et al. 2007). Results pertinent to changes in CE due to aging in smoke plumes are scarce (see
142 discussion in Kleinman et al., 2020). Unfortunately for various reasons, instrument comparisons of measurements of PM1
143 mass loading concentrations were very limited during BBOP, such that there does not exist a useful estimate of a changing
144 CE for either SP-AMS vaporizer with changing plume conditions, so we assume these CEs for the laser on and off modes
145 are to be constant in space and time. We do not attempt to characterize whether the collection efficiency of the SP-AMS
146 changes as the aerosol ages, which is a limitation of this study. This may be a limitation of this study, as collection efficiency
147 has been recently observed to decrease with aging within a laboratory study of biomass burning (Lim et al. 2019). However,
148 no consistent evidence of changing collection efficiencies in field studies exist yet. We use the calculated f_{60} and f_{44}
149 fractions of components (the mass concentrations of m/z 60 and 44 normalized by the total OA mass concentration) and O/C
150 and H/C elemental ratios of OA as tracers of smoke and oxidative aging. Elevated f_{60} values are indicative of
151 “levoglucosan-like” species (levoglucosan and other molecules that similarly fragment in the AMS) (Aiken et al., 2009;
152 Cubison et al., 2011; Lee et al., 2010) and are known to be tracers of smoke primary organic aerosol (POA) (Cubison
153 et al., 2011). The f_{44} the OA fractional component observed by the SP-AMS as the ion fragment (arising from primarily
154 CO_2^+ as well as some acid groups, \Rightarrow) is a proxy for indicative of SOA arising from oxidative aging (Alfarra et al., 2004;
155 Cappa and Jimenez, 2010; Jimenez et al., 2009; Volkamer et al., 2006). Fractional components f_{60} and f_{44} have been shown
156 to decrease and increase with photochemical aging, respectively, likely due to both evaporation and/or oxidation of
157 semivolatile f_{60} -containing species that contribute to m/z 60 in the SP-AMS and addition of oxidized f_{44} -containing species
158 that contribute to m/z 44 in the SP-AMS (Alfarra et al., 2004; Huffman et al., 2009). O/C tends to increase with oxidative
159 aging (Decarlo et al., 2008) whereas H/C ranges from increasing to decreasing with oxidative aging, depending on the types
160 of reactions occurring (Heald et al., 2009). Changes in O/C and H/C (as well as changes in total OA mass, number, f_{44} , and
161 f_{60}) are also influenced by mixing of different air masses and co-oxidation of different VOC precursors (Chen et al. 2015).
162 Tracking H/C with aging may provide clues upon the types of reactions that may be occurring; however, variable oxidation
163 timescales can make inferences of this type difficult (Chen et al. 2015). A Single-Particle Soot Photometer (SP2; Droplet
164 Measurement Technologies) was used to measure refractory black carbon (BC) between 80-500 nm (Schwarz et al. 2010)
165 through laser-induced incandescence (Moteki and Kondo, 2010; Schwarz et al., 2006). An Off-Axis Integrated-Cavity
166 Output Spectroscopy instrument (Los Gatos, Model 907) provided measured CO concentrations measurements. An SPN1
167 radiometer (Badosa et al., 2014; Long et al., 2010) measured provided total shortwave irradiance. Kleinman et al. (2020)
168 provides extensive details for the BBOP instruments used in this work. The supporting information also includes more
169 details on the instruments used.

170 To determine the contribution to the concentration of species X concentrations from smoke emissions (ΔX), the
171 background concentration of X is subtracted off of the measured in-plume species concentrations (ΔX). To correct for

172 dilution, we normalize ΔX by background-corrected CO (ΔCO), which is inert on timescales of near-field aging (Yokelson et
173 al., 2009). Increases or decreases of $\Delta X/\Delta CO$ along the Lagrangian flight path ~~with time~~ indicate whether the total amount of
174 X in the plume has increased or decreased (implying production or removal) since time of emission. The background
175 concentration of X is determined as a regional average of the observed out-of-plume concentrations of X. To avoid using
176 smoke-impacted measurements we apply a threshold of only using measurements of X that occur in regions that correspond
177 to the lowest 10% of CO data. We determine the lowest 10% of CO ~~concentrations data only using from each flight during~~
178 time periods with a similar altitude, latitude, and longitude as the smoke plume ~~in order to exclude flight data taken flying to~~
179 ~~or from each plume.~~ We perform sensitivity calculations on our assumptions of background regions and discuss them in
180 Section 3. ~~We background correct the number size distribution, OA, O, H, C, and BC data in this manner by determining an~~
181 ~~average regional background for each species by using the lowest 10% of the CO data for a given flight with a similar~~
182 ~~altitude, latitude, and longitude as the smoke plume.~~

183 Mass concentrations of Elemental O, H, and C are calculated using the O/C and H/C and OA data from the
184 SP-AMS (assuming all of the OA mass is from O, C, and H), allowing us to calculate ~~the background-corrected OA atomic~~
185 ~~ratios, $\Delta O/\Delta C$, and $\Delta H/\Delta C$, following equation 1 (where X = O or H):~~

$$186 \quad \frac{\Delta X}{\Delta C} = \frac{(X_{in\ plume} - X_{out\ of\ plume})}{(C_{in\ plume} - C_{out\ of\ plume})} \quad \text{Eq. 1}$$

187 We note that any non-linear changes in chemistry and composition between the plume and background will not perfectly
188 isolate the elemental factors in smoke. We also background-correct ~~fractional f_{60} and f_{44} (using the mass concentrations of~~
189 ~~m/z 60, m/z 44, and OA inside and outside of the plume), but we do not normalize by CO due to these values already being~~
190 ~~normalized by OA, following equation 2 (where $f = f_{60}$ or f_{44}):~~

$$191 \quad \Delta f = \frac{(f_{in} * OA_{in}) - (f_{out} * OA_{out})}{\Delta OA} \quad \text{Eq. 2}$$

192 We only consider data to be in-plume if the absolute CO ≥ 150 ppbv, ~~as comparisons of CO and the number concentration~~
193 ~~show that in-plume data has CO ≥ 150 ppbv and out-of-plume (background) data has CO < 150 ppbv.~~ This threshold appears
194 to be capturing clear plume features ~~as seen in the number concentration~~ while excluding background air (Figs. S7-S11). We
195 note that we use different definitions of in-plume and background (~~i.e.~~ the lowest 10% of CO measurements) in order to
196 provide a buffer between the plume and background to ensure to the best of our abilities that we are capturing non-smoke
197 impacted air for the background and smoke-impacted air for in-plume cases. The regions of the lowest 10% of CO
198 measurements always fall under 150 ppbv (Figs. S7-S11). ~~Similarly, we exclude the lowest 5% of CO data in the in-plume~~
199 ~~measurements in our analyses to provide a further buffer between smoke-impacted and background air.~~ We perform
200 sensitivity analyses of our results to our assumptions about background and in-plume values in Section 3. Figures S2-S6
201 indicate the locations of the lowest 10% of CO for each flight.

202 From the FIMS, we examine the background-corrected, normalized number concentrations of particles with
203 mobility diameters between 40-262 nm, $\Delta N/\Delta CO$. This size range allows us to exclude potential influence of fresh
204 nucleation upon the total number concentrations. ~~Occasionally, the background-corrected, normalized number concentration~~

205 in the FIMS size range number concentration between 20-40 nm increases by 1-2 orders of magnitude relative to typical
206 plume conditions, indicating possible nucleation events, primarily at the edges or in between smoke plumes, as the bulk of
207 observed newly formed particles observed fell below 40 nm (Figs. S7-S11). Smoke plumes contain particles with diameters
208 larger than 262 nm (Janhäll et al., 2009); thus and so although, we cannot provide total number concentrations, but, we can
209 infer how the evolution of $\Delta N/\Delta CO$ within our observed size range evolves will impact number concentrations overall. We
210 also obtain an estimate of how the number mean diameter between 40-262 nm, \overline{D}_p , changes with aging through:

211

$$212 \quad \overline{D}_p = \frac{\sum N_i * D_{p,i}}{\sum N_i} \quad \text{Eq. 3}$$

213

214 where N_i and $D_{p,i}$ are the number concentration and geometric mean diameter within each FIMS size bin, respectively.

215 All of the data are provided at 1 Hz and all but the SP-AMS fractional component data are available on the DOE
216 ARM web archive (<https://www.arm.gov/research/campaigns/aaf2013bbop>). As the plane traveled at approximately 100 m
217 s⁻¹ on average, data were collected every 100 m across the plume. The plumes spanned from approximately 5-50 km wide
218 (Figs. S2-6). The instruments used here had a variety of time lags (all <10 seconds) relative to a TSI 3563 nephelometer used
219 as reference. The FIMS also showed additional smearing in flushing smoky air with cleaner air when exiting the plume with
220 maximum observed flushing timescales around 30 seconds, but generally less (Fig. S12). To test if these lags impact our
221 results, we perform an additional analysis where we only consider the first half of each in-plume transect, when
222 concentrations are generally rising with time (Figure S12-S13), and our main conclusions are unaffected. We do not test the
223 impacts of other time lags and do not attempt to further correct the data for any time lags. Kleinman et al. (2020) provides
224 further information on instrument time delays during BBOP.

225 We use MODIS Terra and Aqua fire and thermal anomalies detection data to determine fire locations (Giglio et al.,
226 2006, 2008). We estimate the fire center to be the approximate center of all clustered MODIS detection points for a given
227 sampled fire (Figs. S1-S6). The true fire location at the time of sampling is likely different than the MODIS estimates,
228 depending on the speed of the fire front. To estimate the physical age of the plume, we use the estimated fire center as well
229 as the total FIMS number concentration to determine an approximate centerline of the plume as the smoke travels downwind
230 (an example is provided in Fig. S1). The centerline is subjectively chosen placed to attempt to approximately capture the
231 most-concentrated portion of the total number concentration for each plume pass (as estimated using total aerosol number
232 concentrations), as we focus on aerosol properties and their relations to dilution in this study. We use the mean wind speed
233 and this estimated centerline to calculate an estimated physical age for each transect, and this physical age is assumed to be
234 constant across the transect, as plume crossings took between 50-500 seconds; however, transects that were not perfectly
235 tangential to the mean wind would have sampled different plume ages on the opposite sides of the plume. We did not
236 propagate uncertainty in fire location, wind speed, or centerline through to the physical age, which is a limitation of this
237 study.

238 3 Results and discussion

239 As a case example, we examine the aging profiles of smoke from the Colockum fire during the first set of
240 pseudo-Lagrangian transects ~~for~~ flight 730b (Table S1). Figure 1 provides $\Delta\text{OA}/\Delta\text{CO}$, $\Delta\text{BC}/\Delta\text{CO}$, Δf_{60} , Δf_{44} , $\Delta\text{H}/\Delta\text{C}$,
241 $\Delta\text{O}/\Delta\text{C}$, $\Delta\text{N}/\Delta\text{CO}$, and $\overline{D_p}$ as a function of the estimated physical age; Figs. S14-S18 provides this information for the other
242 pseudo-Lagrangian transect ~~flight~~ sets studied. (Here, BC represents the refractory BC from the SP2; Sect. 2.) We have
243 divided each transect into four regions: between the 5-15 (edge), 15-50 (intermediate, outer), 50-90 (intermediate, inner), and
244 90-100 (core) percentile of ΔCO within each transect. ~~(As discussed above, we~~ We exclude the lowest 5% in order to provide
245 ~~a buffer between the plume edge and background air.) Note that in Figure 1 (and Figures S14-S18), the points represent the~~
246 ~~mean values for each transect/percentile and do not include error bars for uncertainty in the mean or measurement~~
247 ~~uncertainty as characterization of systematic variance (within plume percentiles) with age is beyond the scope of this study~~
248 ~~for figure simplicity.~~ Figures S2-S6 show the locations of these CO percentile bins for each transect of individual flights.
249 Figure 1 shows the edge and core data, both averaged per transect, ~~and~~ while Figs. S14-18 ~~provides~~ providing all four
250 percentile bins for each flight. These percentile bins correspond with the thinnest (~~lowest CO mixing ratio~~ least CO-dense) to
251 thickest (~~highest CO mixing ratio~~ most CO-dense) portions of the plume, respectively. If a fire has uniform emissions ratios
252 across all regions and dilutes evenly downwind, these percentile bins would correspond to the edges, intermediate regions,
253 and the core of the diluting plume. We use this terminology in this study but note that uneven emissions, mixing, and/or
254 dilution lead to the percentile bins not physically corresponding to our defined regions in some cases. We note that some
255 plumes show more than one maxima in CO concentrations within a given plume crossing, which implies that there may be
256 more than one fire or fire front, and that these plumes from separate fires or fronts are not ~~mixing perfectly~~ perfectly-mixing.
257 ~~Multiple maxima could also imply vertical variations in the location of the core of the plumes that the flights did not~~
258 ~~capture.~~ As well, in at least one of the fires (in flights ‘730a’ and ‘730b’), the fuels vary between different sides of the fire,
259 as discussed in Kleinman et al., (2020). However, the lowest two ΔCO bins tend more towards the physical edges of the
260 plume, and the highest two tend more towards the physical center of the plume (Figs. S2-S6). ~~We do not use the data from~~
261 ~~the lowest 5% of ΔCO to reduce uncertainty at the plume-background boundary.~~ We do not know where the plane is
262 vertically in the plume, which is a limitation as vertical location will also impact the amount of solar flux able to penetrate
263 through the plume.

264 Figure 1 shows that for this specific plume, $\Delta\text{OA}/\Delta\text{CO}$ and $\Delta\text{BC}/\Delta\text{CO}$ ~~systematically~~ vary little with age for both
265 the 5-15 and 90-100 percentile of ΔCO (p-values>0.5), ~~yet both show non-systematic variability between transects.~~ A true
266 Lagrangian flight with the aircraft sampling the same portion of the plume and no measurement artifacts (e.g. coincidence
267 errors at high concentrations) would have a constant $\Delta\text{BC}/\Delta\text{CO}$ for each transect ~~set~~. This flight and other flights studied
268 here have ~~slight~~ variations in $\Delta\text{BC}/\Delta\text{CO}$ (Fig. 1; Figs. S14-S18), which may be indicative of deviations from a Lagrangian
269 flight path with temporal variations in emission and/or measurement uncertainties. The remaining variables plotted also
270 show some noise and few clear trends, but it is apparent that the ~~transect-mean values~~ 5-15 and 90-100 percentiles do show a

271 separation for ~~some~~many of the individual metrics, in particular Δf_{44} and $\Delta O/\Delta C$. In order to determine the existence or lack
272 of trends for these metrics, we spend the remainder of this study examining each metric from all of the pseudo-Lagrangian
273 flights together.

274

275 3.1 Organic aerosol aging: $\Delta OA/\Delta CO$, Δf_{60} , Δf_{44} , $\Delta H/\Delta C$, and $\Delta O/\Delta C$

276 Figure 2a-e ~~shows~~show available $\Delta OA/\Delta CO$, Δf_{60} , Δf_{44} , $\Delta H/\Delta C$, and $\Delta O/\Delta C$ edge and core data versus physical age
277 for each transect for each flight of this study. We color each line by the mean ΔOA within a ΔCO percentile bin from the
278 transect closest to the fire, $\Delta OA_{\text{initial}}$, in order to examine whether each variable ($\Delta OA/\Delta CO$, Δf_{60} , Δf_{44} , $\Delta H/\Delta C$, and $\Delta O/\Delta C$)
279 vary with $\Delta OA_{\text{initial}}$. (Some transects do not have data available for specific instruments.) As with Fig. ure 1, the points in
280 Fig. gure 2 represent the mean values for each transect and percentile, and we do not include error bars as we do not attempt
281 to characterize systematic variance (within plume percentiles) with age in this study. ~~that would make the figure unwieldy.~~
282 We note that $\Delta OA_{\text{initial}}$ does not actually represent the true initial emitted OA from each fire, but instead serves as a proxy for
283 the general fire size, intensity, and emission rate (as larger fires and fires with faster rates of fuel consumption per area will
284 have larger mass fluxes than smaller fires or fires with less fuel consumption per area, all else equal) ~~as presumably larger~~
285 ~~fires and fires with faster rates of fuel consumption per area ; more intensely burning fires will have larger mass fluxes than~~
286 ~~smaller, less intensely burning fires~~). Thus, $\Delta OA_{\text{initial}}$ and other “initial” metrics referred to in this study are not to be taken as
287 emission values and direct comparison to studies with direct emissions values is not appropriate, as dilution and chemistry
288 may occur before the initial flight transect, which we discuss further below. We show the 5-15 (edge) and 90-100 (core) ΔCO
289 percentile bins in Fig. 2; Fig. S19 shows the same information for all four ΔCO percentiles. We use the simple ‘edge’ and
290 ‘core’ terminology throughout the following discussion but note that the 5-15 and 90-100 ΔCO percentile bins do not
291 necessarily correspond to the physical (spatial) edges and cores of each plume. They instead correspond to the most
292 CO-dense and least CO-dense portions of the plume. We also note that although some of the physical ages appear to start at
293 approximately 0 hours (e.g. over the fire), this is from a limitation of our physical age estimation method (Sect. 2), as no
294 flights captured data before approximately 15 minutes after emission (Kleinman et al., 2016). Flights with two sets of
295 pseudo-Lagrangian transects (‘726a’ and ‘730b’) have two separate lines in Fig. 2, one for each set. As well, two transects
296 for flight ‘809a’ nearly overlap (Fig. S5), with the transect that is further from the fire occurring first in the flight path,
297 leading to an apparent slight decrease in physical age for the sequential transect (see, e.g., the white dashed line in Fig. 2a).

298 Also included in Fig. 2 are the Spearman rank-order correlation tests (hereafter Spearman tests), which are tests for
299 monotonicity. The Spearman tests show correlation coefficients for each flight set (Table S1) with the initial ΔOA of a flight
300 set ($\Delta OA_{\text{initial}}$) against $\Delta OA/\Delta CO$, Δf_{60} , Δf_{44} , $\Delta H/\Delta C$, and $\Delta O/\Delta C$ as ~~the smoke aerosol ages~~ ~~each variable ages~~ downwind.
301 We also include Spearman tests for the calculated physical age of the smoke for each flight set against these same variables.
302 The R values are labeled $R_{\Delta OA, \text{initial}}$ and R_{age} , respectively, in Fig. 2. ~~We calculate these correlation coefficients separately for~~
303 ~~Figure 2 to determine how well the variability for each variable can be predicted~~ ~~known~~ from the $\Delta OA_{\text{initial}}$ or age alone (and

304 whether the ~~along with if the~~ data are correlated vs. anticorrelated with these predictors). To complement these independent
305 correlation coefficients, we also perform multivariate linear regressions (Eqns. 4 and 5 and Figure 3, discussed later) to
306 explicitly decouple the influence of the two predictors. For the correlations with $\Delta OA_{\text{initial}}$, all transects in a given
307 pseudo-Lagrangian set of transects have the same $\Delta OA_{\text{initial}}$ value; for flights with two pseudo-Lagrangian sets of transects,
308 each set has its own $\Delta OA_{\text{initial}}$ value. Correlating to $\Delta OA_{\text{initial}}$ provides an estimate of how the plume aerosol concentrations at
309 the time of the initial transect impact plume aging (aging both before and after this initial transect). We define the following
310 categories of correlation for the absolute value of R: 0.0-0.19 is 'very weak', 0.2-0.39 is 'weak', 0.4-0.59 is 'moderate',
311 0.6-0.79 is 'strong', and 0.8-1.0 is 'very strong' (Evans 1996).

312 As individual flights show scatter in the metrics of Fig. 2 (Figs. 1, Figs. S14-S18), we also include $R_{\Delta OA, \text{initial}}$ and R_{age}
313 for each metric of Fig. 2 ~~systematically~~ sequentially removing one flight from the statistical analysis. These results are
314 summarized in Table S2. In general, removing single flights does not change our conclusions, particularly when correlations
315 are moderate or stronger. ~~We note that~~ scatter in $\Delta OA_{\text{initial}}$ leads to weaker R_{age} values than would be obtained if we
316 normalized changes with aging to the first (normalized) value. However, as plume-density-dependent aging prior to the first
317 transect is one of the potentially interesting findings of this study, we feel that it is important to not normalize our changes
318 further. Figs. S13, S19-S22 ~~+~~ show the same details as Fig. 2 but provide sensitivity tests ~~to our methodology~~. ~~Figure S13~~
319 ~~uses data from transect portions in which to~~ examines potential FIMS measurement artifacts by only using data from the
320 first 50% of each flight leg when particle concentrations are increasing, which ~~lessons response-time-artifacts of the FIMS~~
321 ~~during transitions from high to low concentration regions. (Fig. S13)~~, Figure S20 tests our assumed in-plume CO threshold
322 value by increasing it from 150 ppbv to 200 ppbv ~~(set to 150 ppbv for Figs. 1-3; Fig. S19-Sect. 2)~~, and Figure S21 tests ΔCO
323 percentile spacing by changing the bins from 5-15%, 15-50%, 50-90%, and 90-100% to 5-25%, 25-75%, and 75-100%.
324 Figure S22 tests assumed background region by increasing data used from the lowest 10% to the lowest 25% of CO
325 measurements. ~~(Figs. S19-S221)~~. Although these figures show slight variability, the findings discussed below remain
326 robust, and we constrain the rest of our discussion to the original assumptions made for the FIMS measurements, in-plume
327 CO threshold value, and ΔCO percentiles used in Fig. 2.

328 In general, both the cores and edges do not show any positive or negative trend in $\Delta OA/\Delta CO$ with ~~respect to~~
329 physical aging. ~~The correlation coefficients, with~~ $R_{\Delta OA, \text{initial}}$ and R_{age} , ~~showing~~ very weak correlations of 0.02 and +0.03
330 (with $R_{\Delta OA, \text{initial}}$ and R_{age} ranging between -0.25 to +0.17 and 0 to 0.07, respectively, when individual flights are left out
331 sequentially; Table S2). The absolute variability in $\Delta OA/\Delta CO$ is dominated by differences between plumes. ~~Many previous~~
332 ~~field campaigns similarly show little change in $\Delta OA/\Delta CO$ with aging (Hodshire et al., 2019a and references therein; Palm et~~
333 ~~al., 2020). This may be due to a balance between evaporation and condensation over the period of time that the plume is~~
334 ~~observed (Hodshire et al., 2019a), rapid chemistry leading to SOA enhancements prior to the time of the first measurement~~
335 ~~that d~~ This hypothesis is supported by the observed Δf_{60} and Δf_{44} . ~~While the observed trends in $\Delta OA/\Delta CO$ with aging are~~
336 ~~small,~~ The fractional components Δf_{60} and Δf_{44} show clear signs of changes with aging, consistent with previous studies
337 ~~(Cubison et al. 2011; May et al. 2015; Garofalo et al. 2019; Forrister et al. 2015; Lee et al. 2020) (Cubison et al., 2011;~~

338 ~~Carofalo et al., 2019; May et al., 2015).~~ Δf_{60} generally decreases with plume age ($R_{\text{age}} = -0.26$; a weak correlation), consistent
339 with the hypotheses that ~~compounds containing species that can fragment to m/z 60~~ Δf_{60} in the SP-AMS may be evaporating
340 because of dilution, undergoing heterogeneous oxidation to new forms that do not appear at m/z 60, and/or having a
341 decreasing fractional contribution due to condensation of other compounds. In contrast, Δf_{44} generally increases with age
342 ($R_{\text{age}} = +0.5$; a moderate correlation) for all plumes with available data. It appears for the plumes in this study that although
343 there is little change in $\Delta\text{OA}/\Delta\text{CO}$, loss of compounds ~~such as those that contribute to that contain~~ f_{60} fragments (as captured
344 by the SP-AMS) is roughly balanced by condensation of more-oxidized compounds, including those that contain compounds
345 with f_{44} fragments, such as carboxylic acids. This observation also suggests the possibility of heterogeneous or particle-phase
346 oxidation that would alter the balance of Δf_{60} and Δf_{44} . However, estimates of heterogeneous mass losses indicate that after
347 three hours of aging (~~the range of time the BBOP measurements were taken in~~) for a range of OH concentrations and
348 reactive uptake coefficients, ~~less than 10% of aerosol mass is lost to heterogeneous reactions (Fig. S23; see SI text S2 for~~
349 ~~more details on the calculation).~~ ~~over 90% of aerosol mass is anticipated to remain.~~ These calculations indicating that
350 heterogeneous loss has limited effect on aerosol composition or mass (~~Fig. S23; see SI text S2 for more details on the~~
351 ~~calculation).~~ Hence, the evaporation of ~~compounds that contribute to m/z 60 in the SP-AMS containing~~ f_{60} fragments being
352 balanced by gas-phase production of ~~compounds that contribute to m/z 44 in the SP-AMS containing~~ f_{44} fragments may be
353 the more likely pathway. When individual flights are left out sequentially, R_{age} ranges from -0.21 to -0.38 and +0.4 to +0.57
354 for Δf_{60} and Δf_{44} , respectively (Table S2).

355 Two more important features of Δf_{60} and Δf_{44} can be seen within Fig. 2: (1) Δf_{60} and Δf_{44} depend on $\Delta\text{OA}_{\text{initial}}$
356 (moderate correlations of $R_{\Delta\text{OA,initial}} = +0.43$ and -0.55 , respectively), ~~with plumes with higher $\Delta\text{OA}_{\text{initial}}$ with more~~
357 ~~concentrated plumes~~ having consistently higher Δf_{60} and lower Δf_{44} . (2) ~~The differences in Δf_{60} and Δf_{44} are apparent even~~
358 ~~for the nearest-to-source measurements that are ~15 minutes after the time of emission. indicate that evaporation and/or~~
359 ~~chemistry appears to have likely occurred before the time of these first measurements. (assuming that emitted Δf_{60} and Δf_{44} at~~
360 ~~the time of emission do not correlate with $\Delta\text{OA}_{\text{initial}}$; there is currently no evidence for this alternative hypothesis).~~ Prior
361 studies have shown that f_{60} and f_{44} at the time of emissions correlate with OA emissions factors through variability in burn
362 conditions (Hennigan et al. 2011; Cubison et al. 2011; McClure et al. 2020), and this relationship might also contribute to our
363 observed correlation between Δf_{60} and Δf_{44} with $\Delta\text{OA}_{\text{initial}}$, ~~however, if~~ for this emissions relationship to be an important
364 factor, the variability in the OA emission factor needs to be a significant contributor to the variability in $\Delta\text{OA}_{\text{initial}}$. ~~(If~~
365 ~~the relative variability in the OA emission factor is much smaller than the relative variability in $\Delta\text{OA}_{\text{initial}}$, other factors~~
366 ~~contributing to variability in $\Delta\text{OA}_{\text{initial}}$ will negate and wash out this emissions-based covariance between $\Delta\text{OA}_{\text{initial}}$ with Δf_{60}~~
367 ~~and Δf_{44}).~~ While our observed $\Delta\text{OA}_{\text{initial}}$ in Figure 2 spans nearly a factor of 100, Andreae (2019) shows that the OA emission
368 factors have a -1σ to $+1\sigma$ range of around a factor 3. Hence, variability in fuel consumption rates and dilution prior to the
369 first transect likely dominate the variability in $\Delta\text{OA}_{\text{initial}}$, and the relationships of Δf_{60} and Δf_{44} with $\Delta\text{OA}_{\text{initial}}$ are unlikely to be
370 influenced much by variability in burn conditions. ~~We conclude that~~ Hence, evaporation and/or chemistry prior to the first
371 measurement appears to drive the initial relationship between Δf_{60} and Δf_{44} with $\Delta\text{OA}_{\text{initial}}$, consistent with (1) the theoretical

372 work of Hodshire et al. (2019a), (2) an analysis of what chemistry would be missed in laboratory experiments if the initial
373 10-60 minutes of chemistry was not considered, following field experiments (Hodshire et al., 2019b), and (3) the recent field
374 analysis indicating that up to one-third of primary OA from biomass burning evaporates and subsequently reacts to form
375 biomass burning SOA (Palm et al. 2020) (Palm et al., 2020). We include in the supporting information scatter plots of each
376 parameter of Fig. 1 as a function of $\Delta\text{OA}_{\text{initial}}$ (Fig. S24), and observe no trends other than the cores of the plumes generally
377 having a higher $\Delta\text{OA}_{\text{initial}}$ than the edges of the plumes, as expected. The amounts of evaporation and/or chemistry appear to
378 depend on $\Delta\text{OA}_{\text{initial}}$, with higher rates of evaporation and chemistry occurring for lower values of $\Delta\text{OA}_{\text{initial}}$. This result is
379 consistent with the hypothesis that aircraft observations are missing evaporation and chemistry prior to the first aircraft
380 observation (Hodshire et al., 2019b). The differences in $\Delta\text{OA}_{\text{initial}}$ between plumes may be due to different emissions fluxes
381 (e.g., due to different fuels or combustion phases) or plume widths, where larger/thicker plumes dilute more slowly than
382 smaller/thinner plumes. These larger plumes have been predicted to have less evaporation and may undergo relatively less
383 photooxidation (Bian et al., 2017; Hodshire et al., 2019a, 2019b). We note that each fire may emit particles with variable
384 initial f_{44} and f_{60} values, as has been observed in laboratory studies (Hennigan et al. 2011; Cubison et al. 2011; McClure et al.
385 2020), which adds to scatter within the data. It is possible that variability in f_{44} and f_{60} emissions may also contribute to the
386 observed correlations with $\Delta\text{OA}_{\text{initial}}$, however, this would require that higher f_{44} emissions of species able to contribute to m/z
387 44 are correlated with lower emissions rates and/or faster dilution rates (and vice versa for species able to contribute to m/z
388 60 f_{60}). Lacking direct emissions measurements, this hypothesis cannot be further explored in this work. When individual
389 flights are left out sequentially, $R_{\Delta\text{OA},\text{initial}}$ ranges from +0.3 to +0.58 and -0.42 to -0.63 for Δf_{60} and Δf_{44} , respectively (Table
390 S2).

391 Garofalo et al. (2019) segregated smoke data from the WE-CAN field campaign by distance from the center of a
392 given plume and showed that the edges of one of the fires studied have less fractional f_{60} and more fractional f_{44} (not
393 background-corrected) than the core of the plume. Lee et al. (2020) saw similar patterns in a southwestern United States
394 wildfire. Similarly, we find that the 730b flight shows a very similar pattern in f_{60} and f_{44} (Figs. S254-S265) to that shown in
395 Fig. 6 of Garofalo et al. (2019). The 821b and 809a flights also hint at elevated f_{44} and decreased f_{60} at the edges but the
396 remaining plumes do not show a clear trend from the physical edges to cores in f_{60} and f_{44} . This could be as CO
397 concentrations (and thus presumably other species) do not evenly increase from the edge to the core for many of the plume
398 transects studied (Figs. S2-S6). To more clearly see this, Fig. S27 provides the same style of figure as Figs. S26-S27 for
399 in-plume CO concentrations. Generally CO peaks around the centerline and is highest in the most fresh transect, but shows
400 variability across transects. We do not have UV measurements that allow us to calculate photolysis rates but the in-plume
401 SPN1 shortwave measurements in the visible show a dimming in the fresh cores that has a similar pattern to f_{44} and the
402 inverse of f_{60} (Fig. S28; the rapid oscillations in this figure could be indicative of sporadic cloud cover above the plumes).
403 Lee et al. (2020) similarly saw indications of enhanced photochemical bleaching at the edges of a southwestern United States
404 wildfire when examining aerosol optical properties.

405 We also plot core and edge $\Delta\text{H}/\Delta\text{C}$ and $\Delta\text{O}/\Delta\text{C}$ as a function of physical age (Fig. 2d-e). Similar to Δf_{44} , $\Delta\text{O}/\Delta\text{C}$
 406 increases with physical age and is well correlated to both physical age and $\Delta\text{OA}_{\text{initial}}$ (moderate correlations of $R_{\text{age}} = +0.561$
 407 and $R_{\Delta\text{OA},\text{initial}} = -0.45$). When individual flights are left out sequentially, R_{age} for $\Delta\text{O}/\Delta\text{C}$ ranges between +0.46 and +0.63 and
 408 $R_{\Delta\text{OA},\text{initial}}$ ranges between -0.21 and -0.54 (Table S2). Given that Δf_{44} and $\Delta\text{O}/\Delta\text{C}$ are both metrics for OA aging (Sect. 2), it is
 409 unsurprising that we see similar trends between them. Conversely, $\Delta\text{H}/\Delta\text{C}$ ~~tends to be fairly constant or slightly decreasing~~
 410 ~~with physical age and is~~ poorly correlated to physical age and $\Delta\text{OA}_{\text{initial}}$. ~~A Van Krevelen diagram of $\Delta\text{H}/\Delta\text{C}$ versus $\Delta\text{O}/\Delta\text{C}$~~
 411 ~~(Fig. S27) indicates that oxygenation reactions or a combination of oxygenation and hydration reactions are likely dominant~~
 412 ~~(Heald et al., 2010) (recalling that $\Delta\text{H}/\Delta\text{C}$ and $\Delta\text{O}/\Delta\text{C}$ are calculated by background-correcting the individual elements~~
 413 ~~before ratioing; Eq. 1); however, without further information, we cannot conclude which reactions are occurring.~~

414 Both physical age and $\Delta\text{OA}_{\text{initial}}$ appear to influence Δf_{60} , Δf_{44} , and $\Delta\text{O}/\Delta\text{C}$: oxidation reactions and evaporation
 415 ~~promoted by~~ ~~from~~ dilution occur with aging, and the extent of photochemistry and dilution should depend on plume
 416 thickness. Being able to predict biomass burning aerosol aging parameters can provide a framework for
 417 interstudy-comparisons and can aid in modeling efforts. We construct mathematical fits for predicting Δf_{60} , Δf_{44} , and $\Delta\text{O}/\Delta\text{C}$:
 418

$$419 \quad X = a \log_{10}(\Delta\text{OA}_{\text{initial}}) + b (\text{Physical age}) + c \quad \text{Eq. 4}$$

420
 421 where X is Δf_{60} , Δf_{44} , or $\Delta\text{O}/\Delta\text{C}$, physical age is in hours, and a , b , and c are fit coefficients. The measured versus fit data are
 422 shown in Fig. 3a-c. The values of a , b , and c are provided in Table S3. The Pearson and Spearman coefficients of
 423 determination (R_p^2 and R_s^2 , respectively) are also summarized in Fig. 3 and indicate weak-moderate goodness of fits (R_p^2 and
 424 R_s^2 of 0.28 and 0.25 for Δf_{60} , R_p^2 and R_s^2 of 0.58 and 0.6 for Δf_{44} , and R_p^2 and R_s^2 of 0.45 and 0.55 for $\Delta\text{O}/\Delta\text{C}$). We show R^2
 425 here to indicate the fraction of variability captured by these fits, whereas calculating R for the trends in Fig. 2 indicate the
 426 direction of the correlation. We do not constrain our fits to go through the origin. To provide further metrics of
 427 goodness-of-fit, we also include the normalized mean bias (NMB) and normalized mean error (NME) in percent for each
 428 metric of Fig. 3. The NMB values are very close to zero (which is anticipated as linear fits seek to minimize the sum of
 429 squared residuals). The NME is ~~larger~~ ~~more variable~~, at 19.8% for Δf_{60} , 14.9% for Δf_{44} , and 10.2% for $\Delta\text{O}/\Delta\text{C}$. The p-values
 430 for each fit ~~are~~ less than 0.01. Although no models that we are aware of currently predict aerosol fractional components
 431 (e.g. f_{60} or f_{44}), O/H and H/C are predicted by some models (e.g., ~~(Cappa and Wilson, (2012)~~ and these fit parameters may
 432 assist in ~~biomass burning~~ modeling of aging biomass burning aerosol emissions. ~~¶~~
 433 Other functional forms for fits were explored, with the following form showing similar results as Eq. 4:

$$434$$

$$435 \quad \ln(\Delta X) = a \ln(\Delta\text{OA}_{\text{initial}}) + b \ln(\text{Physical age}) + c \quad \text{Eq. 5}$$

436

437 (Fig. S298 and Table S4 for the fit coefficients) and $\Delta N_{\text{initial}}$ in the place of $\Delta \text{OA}_{\text{initial}}$ in Eq. 4 (Fig. S3029 and Table S5 for the
438 fit coefficients) providing similar correlation values and NMB and NME values for Δf_{60}^* , Δf_{44}^* , and $\Delta \text{O}/\Delta \text{C}$.

439 The aging values of Δf_{60}^* , Δf_{44}^* , and $\Delta \text{O}/\Delta \text{C}$ show scatter (Figs. S14-18), which likely contributes to the limited
440 predictive power of our mathematical fits. The scatter is likely due to variability in emissions due to source fuel or
441 combustion conditions, instrument noise and responses under the large concentration ranges encountered in these smoke
442 plumes, inhomogeneous mixing within the plume, variability in background concentrations not captured by our background
443 correction method, inaccurate characterizations of physical age due to variable wind speed, and/or deviations from a true
444 Lagrangian flight path. Eqs. 4-5 performed the best out of the mathematical fits that we tested. These equations do not have a
445 direct physical interpretation but may be used as a starting point for modeling studies as well as for constructing a more
446 physically based fit. There may be another variable not available to us in the BBOP measurements that can improve these
447 mathematical fits, such as photolysis rates. We do not know whether these fits may well-represent fires in other regions
448 around the world, given variability in fuels and burn conditions. We also do not know how these fits will perform under
449 nighttime conditions, as our fits were made ~~for~~during daytime conditions with different chemistry than would happen at
450 night. We encourage these fits to be tested with further data sets and modeling. These equations are a first step towards
451 parameterizations appropriate for regional and global modeling and need extensive testing to separate influences of oxidation
452 versus dilution-driven evaporation.

453 3.2 Aerosol size distribution properties: $\Delta \text{N}/\Delta \text{CO}$ and \overline{D}_p

454 The observations of the normalized number concentration between 40-262 nm, $\Delta \text{N}/\Delta \text{CO}$ (Fig. 2f), show that plume
455 edges and cores generally show decreases in $\Delta \text{N}/\Delta \text{CO}$ with physical age, with a weak correlation of $R_{\text{age}} = -0.27$ (-0.13 to
456 -0.43 when individual flights are left out, sequentially; Table S2). Although we would anticipate that plume regions with
457 higher initial ΔOA would have lower normalized number concentrations due to coagulation ([Sakamoto et al. 2016](#)), a few
458 dense cores have normalized number concentrations comparable or higher than the thinner edges, leading to no correlation
459 with $\Delta \text{OA}_{\text{initial}}$. We note that variability in number emissions (e.g., due to ~~e.g.~~ burn conditions) adds unexplained variability
460 not captured by the R values.

461 The mean particle size between 40-262 nm, \overline{D}_p (Eq. 3), is shown to statistically increase with aging when
462 considered across the BBOP dataset (Fig. 2g) (a moderate correlation of $R_{\text{age}} = +0.53$, with R_{age} ranging between +0.43 to
463 +0.63 when individual flights are left out sequentially; Table S2). Coagulation and SOA condensation will increase \overline{D}_p . OA
464 evaporation will decrease \overline{D}_p if the particles are in quasi-equilibrium (where evaporation is independent of surface area)
465 ([Hodshire et al. 2019b](#)). However, if evaporation is kinetically limited, smaller particles will preferentially evaporate more
466 rapidly than larger particles, which may lead to an increase in \overline{D}_p if the smallest particles evaporate below 40 nm ([Hodshire
467 et al. 2019b](#)). The plumes do not show significant changes in $\Delta \text{OA}/\Delta \text{CO}$ (Fig. 2a), indicating that coagulation is likely

468 responsible for the majority of increases in $\overline{D_p}$. (We acknowledge that $\Delta OA/\Delta CO$ may be impacted by measurement
469 artifacts as discussed in Sect. 2. For instance, if the collection efficiency of the AMS is actually decreasing with age, then
470 $\Delta OA/\Delta CO$ would be increasing and the increases in **number** mean diameter will be due to SOA condensation as well as
471 coagulation.) We do not have measurements for the volatility of the smoke aerosol, and so cannot refine these conclusions
472 further. We also perform the functional fit analysis following Sect. 3.1 (Eq. 4; where X is $\overline{D_p}$ in this case). The fit can also
473 predict greater than 30 percent of the variance in $\overline{D_p}$ (R_p^2 and R_s^2 of 0.37 and 0.33, NME of 5.5%, and p-value less than
474 0.01; Fig. 3d) but does not ~~well~~-predict $\Delta N/\Delta CO$ **well** (not shown). We show the functional fit for $\overline{D_p}$ for the alternative fit
475 equation (Eq. 5) in Fig. S29~~8~~ and Table S4. We also show the functional fit for $\overline{D_p}$ for Eq. 4 with $\Delta N_{\text{initial}}$ in place of
476 $\Delta OA_{\text{initial}}$ in Fig. 3029~~9~~ and Table S5. Sakamoto et al. (2016) provide fit equations for modeled $\overline{D_p}$ as a function of age, but
477 they include a known initial $\overline{D_p}$ at the time of emission in their parameterization (rather than 15 minutes or greater, as
478 available to us in this study), which is not available here. $\Delta N_{\text{initial}}$ in the place of $\Delta OA_{\text{initial}}$ in Eq. 4 predicts $\overline{D_p}$ similarly (Fig.
479 S3029~~9~~). As discussed in Section 3.1, scatter in number concentrations limits our prediction skill.

480 **Particles appear in the 20-40 nm size range in the FIMS measurements independently of plume OA concentrations**
481 **(Figs S7-S11), implying that nucleation events may be occurring.** ~~Nucleation-mode particles (inferred in this study from~~
482 ~~particles appearing between 20-40 nm in the FIMS measurements) are observed~~ for some of the transects (S7-S11). Some
483 pseudo-Lagrangian sets of transects also show nucleation-mode particles downwind of fires in between transects (Figs. S7,
484 S8, S9, and S11). Nucleation-mode particles appear to be approximately one order of magnitude less concentrated than the
485 larger particles, and primarily occur in the outer portion of plumes, although one **set of transects**~~day~~ did show
486 nucleation-mode particles within the core of the plume (Fig. S11). Nucleation at edges could be due to increased
487 photooxidation from higher total irradiance relative to the core (Fig. S26). As well, nucleation is more favorable when the
488 total condensation sink is lower (e.g. reduced particle surface area; Dal Maso et al., 2002), which may occur for outer
489 portions of plumes with little aerosol loading. However, given the relatively small number of data points showing nucleation
490 mode particles and limited photooxidation and gas-phase information, we do not have confidence in the underlying source of
491 the nucleation-mode particles.

492 **4 Summary and outlook**

493 The BBOP field campaign provided high time resolution (1 s) measurements of gas- and particle-phase smoke
494 measurements downwind of western U.S. wildfires along pseudo-Lagrangian transects. These flights have allowed us to
495 examine near-field (<4 hours) aging of smoke particles to provide analyses on how **select these** species vary across a range
496 of initial **organic** aerosol mass loadings ($\Delta OA_{\text{initial}}$; a proxy for the relative rates at which the plume is anticipated to dilute as
497 dilution before the first observation is not a measurable quantity) as well as how the **species studied**~~y~~ vary between the edges

498 and cores of each plume. We find that although $\Delta\text{OA}/\Delta\text{CO}$ does not correlate with $\Delta\text{OA}_{\text{initial}}$ or physical age, Δf_{60} (a marker
499 for evaporation) is moderately correlated with $\Delta\text{OA}_{\text{initial}}$ (Spearman rank-order correlation tests correlation coefficient,
500 $R_{\Delta\text{OA,initial}}$ of +0.43) and weakly correlated with physical age (Spearman rank-order correlation tests correlation coefficient,
501 R_{age} of -0.26). Δf_{44} and $\Delta\text{O}/\Delta\text{C}$ (markers for photochemical aging) increases with physical aging (moderate correlations of
502 R_{age} of +0.5 and +0.56, respectively) and are inversely related to $\Delta\text{OA}_{\text{initial}}$ (moderate correlations of $R_{\Delta\text{OA,initial}}$ of -0.55 and
503 -0.45, respectively). $\Delta\text{N}/\Delta\text{CO}$ likely decreases with physical aging, likely through coagulation. Mean aerosol diameter
504 increases with age primarily due to coagulation, as organic aerosol mass does not change significantly, and is moderately
505 correlated with physical age ($R_{\text{age}} = +0.53$). Nucleation is observed within a few of the fires and appears to occur primarily
506 on the edges of the plumes. Differences in initial values of Δf_{60} , Δf_{44} , and $\Delta\text{O}/\Delta\text{C}$ ~~between higher and lower concentrated~~
507 ~~plumes are evidence indicate~~ that evaporation and/or chemistry has likely occurred before the time of initial measurement and
508 that plumes or plume regions ~~(such as the outer parts of the plume)~~ with lower initial aerosol loading can undergo these
509 changes more rapidly than thicker plumes. We have developed fit equations that can weakly to moderately predict Δf_{60} , Δf_{44} ,
510 $\Delta\text{O}/\Delta\text{C}$, and mean aerosol diameter given a known initial (at the time of first measurement) total organic aerosol mass
511 loading and physical age. We were unable to quantify the impact on potential inter-fire variability in the emission values of
512 the metrics studied here (such as variable emissions of ~~species that can contribute to m/z 60 f_{60} and m/z 44 f_{44}~~). We anticipate
513 that being able to capture this additional source of variability may lead to stronger fits and correlation. We encourage future
514 studies to attempt to quantify these chemical and physical changes before the initial measurement using combinations of
515 modeling and laboratory measurements, where sampling is possible at the initial stages of the fire and smoke. We also
516 suggest further refinement of our fit equations, as ~~additional further~~ variables (such as photolysis rates) and better
517 quantification of inter-fire variability (such as variable emission rates) are anticipated to improve these fits. We finally urge
518 future near-field (<24 hours) analyses of recent and future biomass burning field campaigns to include differences in initial
519 plume mass concentrations and location within the plume as considerations for understanding chemical and physical
520 processes in plumes.

521 **Acknowledgements**

522 We would like to thank Lauren Garofalo, Emily Fischer, Jakob Lindaas, and Ilana Pollack for useful conversations. We thank
523 Charles Long for use of irradiation data. This work is supported by the U.S. NOAA, an Office of Science, Office of
524 Atmospheric Chemistry, Carbon Cycle, and Climate Program, under the cooperative agreement awards NA17OAR4310001
525 and NA17OAR4310003; the U.S. NSF Atmospheric Chemistry program, under Grants AGS-1559607 and AGS-1950327;
526 and the US Department of Energy's (DOE) Atmospheric System Research, an Office of Science, Office of Biological and
527 Environmental Research program, under grant DE-SC0019000. Work conducted by LIK, AJS, JW was performed under
528 sponsorship of the U.S. DOE Office of Biological & Environmental Sciences (OBER) Atmospheric System Research
529 Program (ASR) under contracts DE-SC0012704 (BNL; LIK, AJS) and DE-SC0020259 (JW). Researchers recognize the

530 DOE Atmospheric Radiation Measurement (ARM) Climate Research program and facility for both the support to carry out
531 the BBOP campaign and for use of the G-1 research aircraft. TBO acknowledges support from the DOE ARM program
532 during BBOP and the DOE ASR program for BBOP analysis (contract DE-SC0014287). DKF acknowledges funding from
533 NOAA Climate Program Office's Atmospheric Chemistry, Carbon Cycle, and Climate program (Grant NA17OAR4310010).
534 [We thank the anonymous reviewers for their constructive feedback.](#)

535

536

537

538 **References**

- 539 Adachi, K., Sedlacek, A. J., Kleinman, L., Springston, S. R., Wang, J. and Chand, D.: Spherical tarball particles form
540 through rapid chemical and physical changes of organic matter in biomass-burning smoke, *Proceedings of the*
541 *National Academy of Sciences*, 1–6, 2019.
- 542 Aiken, A. C., Decarlo, P. F., Kroll, J. H., Worsnop, D. R., Huffman, J. A., Docherty, K. S., Ulbrich, I. M., Mohr, C., Kimmel,
543 J. R., Sueper, D., Sun, Y., Zhang, Q., Trimborn, A., Northway, M., Ziemann, P. J., Canagaratna, M. R., Onasch, T.
544 B., Alfarra, M. R., Prevot, A. S. H., Dommen, J., Duplissy, J., Metzger, A., Baltensperger, U. and Jimenez, J. L.:
545 O/C and OM/OC ratios of primary, secondary, and ambient organic aerosols with high-resolution time-of-flight
546 aerosol mass spectrometry, *Environmental Science and Technology*, 42(12), 4478–4485, 2008.
- 547 Aiken, A. C., Salcedo, D., Cubison, M. J., Huffman, J. A., DeCarlo, P. F., Ulbrich, I. M., Docherty, K. S., Sueper, D.,
548 Kimmel, J. R., Worsnop, D. R. and Others: Mexico City aerosol analysis during MILAGRO using high resolution
549 aerosol mass spectrometry at the urban supersite (T0)--Part 1: Fine particle composition and organic source
550 apportionment, *Atmos. Chem. Phys.*, 9(17), 6633–6653, 2009.
- 551 Akagi, S. K., Yokelson, R. J., Wiedinmyer, C., Alvarado, M. J., Reid, J. S., Karl, T., Crouse, J. D. and Wennberg, P. O.:
552 Emission factors for open and domestic biomass burning for use in atmospheric models, *Atmos. Chem. Phys.*,
553 11(9), 4039–4072, 2011.
- 554 Akagi, S. K., Craven, J. S., Taylor, J. W., Mcmeeking, G. R., Yokelson, R. J., Burling, I. R., Urbanski, S. P., Wold, C. E.,
555 Seinfeld, J. H., Coe, H., Alvarado, M. J. and Weise, D. R.: Evolution of trace gases and particles emitted by a
556 chaparral fire in California, *Atmos. Chem. Phys.*, 12, 1397–1421, 2012.
- 557 Albrecht, B. A.: Aerosols, cloud microphysics, and fractional cloudiness, *Science*, 245(4923), 1227–1230, 1989.

558 Alfarra, M. R., Coe, H., Allan, J. D., Bower, K. N., Boudries, H., Canagaratna, M. R., Jimenez, J. L., Jayne, J. T., Garforth,
559 A. A., Li, S.-M. and Worsnop, D. R.: Characterization of urban and rural organic particulate in the Lower Fraser
560 Valley using two Aerodyne Aerosol Mass Spectrometers, *Atmos. Environ.*, 38(34), 5745–5758, 2004.

561 Andela, N., Morton, D. C., Giglio, L., Paugam, R., Chen, Y., Hantson, S., Werf, G. R. and Randerson, J. T.: The Global Fire
562 Atlas of individual fire size, duration, speed and direction, *Earth System Science Data*, 11(2), 529–552, 2019.

563 [Andreae, M. O.: Emission of trace gases and aerosols from biomass burning – an updated assessment, *Atmos. Chem. Phys.*,
564 19, 8523–8546, <https://doi.org/10.5194/acp-19-8523-2019>, 2019.](#)

565 Badosa, J., Wood, J., Blanc, P., Long, C. N., Vuilleumier, L., Demengel, D. and Haeffelin, M.: Solar irradiances measured
566 using SPN1 radiometers: uncertainties and clues for development, *Atmospheric Measurement Techniques*, 7,
567 4267–4283, 2014.

568 Bian, Q., Jathar, S. H., Kodros, J. K., Barsanti, K. C., Hatch, L. E., May, A. A., Kreidenweis, S. M. and Pierce, J. R.:
569 Secondary organic aerosol formation in biomass-burning plumes: Theoretical analysis of lab studies and ambient
570 plumes, *Atmos. Chem. Phys.*, 17(8), 5459–5475, 2017.

571 Brito, J., Rizzo, L. V., Morgan, W. T., Coe, H., Johnson, B., Haywood, J., Longo, K., Freitas, S., Andreae, M. O. and Artaxo,
572 P.: Ground-based aerosol characterization during the South American Biomass Burning Analysis (SAMBBA) field
573 experiment, *Atmospheric Chemistry and Physics*, 14(22), 12069–12083, doi:10.5194/acp-14-12069-2014, 2014.

574 Cachier, H., Liousse, C., Buat-Menard, P. and Gaudichet, A.: Particulate content of savanna fire emissions, *J. Atmos. Chem.*,
575 22(1-2), 123–148, 1995.

576 Canagaratna, M. R., Jimenez, J. L., Kroll, J. H., Chen, Q., Kessler, S. H., Massoli, P., Hildebrandt Ruiz, L., Fortner, E.,
577 Williams, L. R., Wilson, K. R. and Others: Elemental ratios measurements of organic compounds using aerosol
578 mass spectrometry: characterization, improved calibration, and implications, *Atmos. Chem. Phys.*, 15, 253–272,
579 2015.

580 Capes, G., Johnson, B., McFiggans, G., Williams, P. I., Haywood, J. and Coe, H.: Aging of biomass burning aerosols over
581 West Africa: Aircraft measurements of chemical composition, microphysical properties, and emission ratios, *J.*
582 *Geophys. Res. D: Atmos.*, 113(23), 0–15, 2008.

583 Cappa, C. D. and Jimenez, J. L.: Quantitative estimates of the volatility of ambient organic aerosol, *Atmos. Chem. Phys.*,
584 10(12), 5409–5424, 2010.

585 Cappa, C. D. and Wilson, K. R.: Multi-generation gas-phase oxidation, equilibrium partitioning, and the formation and
586 evolution of secondary organic aerosol, *Atmos. Chem. Phys.*, 12(20), 9505–9528, 2012.

587 Carrico, C. M., Petters, M. D., Kreidenweis, S. M., Collett, J. L., Jr., Engling, G. and Malm, W. C.: Aerosol hygroscopicity
588 and cloud droplet activation of extracts of filters from biomass burning experiments, *J. Geophys. Res.*, 113(D8),
589 4767, 2008.

590 Canagaratna, M., Jayne, J., Jimenez, J., Allan, J., Alfarra, M., Zhang, Q., Onasch, T., Drewnick, F., Coe, H., Middlebrook,
591 A., Delia, A., Williams, L., Trimborn, A., Northway, M., DeCarlo, P., Kolb, C., Davidovits, P. and Worsnop, D.:

592 Chemical and microphysical characterization of ambient aerosols with the aerodyne aerosol mass spectrometer,
593 Mass Spectrom. Rev., 26: 185-222. doi:10.1002/mas.20115, 2007

594
595
596
597
598

599 Chen, Q., Heald, C. L., Jimenez, J. L., Canagaratna, M. R., Qi, Z., Ling-Yan, H., Xiao-Feng, H., Campuzano-Jost, P., Palm,
600 B. B., Poulain, L., Kuwata, M., Martin, S. T., Abbatt, J. P. D., Lee, A. K. Y., and Liggio, J.: Elemental composition
601 of organic aerosol: the gap between ambient and laboratory measurements, Geophysical Research Letters, 42,
602 4182-4189, <https://doi.org/10.1002/2015gl063693>, 2015

603 Collier, S., Zhou, S., Onasch, T. B., Jaffe, D. A., Kleinman, L., Sedlacek, A. J., Briggs, N. L., Hee, J., Fortner, E., Shilling, J.
604 E., Worsnop, D., Yokelson, R. J., Parworth, C., Ge, X., Xu, J., Butterfield, Z., Chand, D., Dubey, M. K., Pekour, M.
605 S., Springston, S. and Zhang, Q.: Regional Influence of Aerosol Emissions from Wildfires Driven by Combustion
606 Efficiency: Insights from the BBOP Campaign, Environmental Science and Technology, 50(16), 8613–8622, 2016.

607 Collier, S., Williams, L. R., Onasch, T. B., Cappa, C. D., Zhang, X., Russell, L. M., Chen, C. L., Sanchez, K. J., Worsnop, D.
608 R. and Zhang, Q.: Influence of Emissions and Aqueous Processing on Particles Containing Black Carbon in a
609 Polluted Urban Environment: Insights From a Soot Particle-Aerosol Mass Spectrometer, J. Geophys. Res. Atmos.,
610 123(12), 6648–6666, doi:10.1002/2017JD027851, 2018.

611 Corbin, J. C., Lohmann, U., Sierau, B., Keller, A., Burtscher, H., and Mensah, A. A.: Black carbon surface oxidation and
612 organic composition of beech-wood soot aerosols, Atmos. Chem. Phys., 15, 11885–11907,
613 <https://doi.org/10.5194/acp-15-11885-2015>, 2015.

614 Cubison, M. J., Ortega, A. M., Hayes, P. L., Farmer, D. K., Day, D., Lechner, M. J., Brune, W. H., Apel, E., Diskin, G. S.,
615 Fisher, J. A., Fuelberg, H. E., Hecobian, A., Knapp, D. J., Mikoviny, T., Riemer, D., Sachse, G. W., Sessions, W.,
616 Weber, R. J., Weinheimer, A. J., Wisthaler, A. and Jimenez, J. L.: Effects of aging on organic aerosol from open
617 biomass burning smoke in aircraft and laboratory studies, Atmos. Chem. Phys., 11(23), 12049–12064, 2011.

618 Dal Maso, M., Kulmala, M., Lehtinen, K. E. J., Mäkelä, J. M., Aalto, P., and O'Dowd, C. D.: Condensation and coagulation
619 sinks and formation of nucleation mode particles in coastal and boreal forest boundary layers, J. Geophys. Res.,
620 107(D19), doi:[10.1029/2001JD001053](https://doi.org/10.1029/2001JD001053), 2002.

621 Decarlo, P. F., Dunlea, E. J., Kimmel, J. R., Aiken, A. C., Sueper, D., Crouse, J., Wennberg, P. O., Emmons, L., Shinozuka,
622 Y., Clarke, A., Zhou, J., Tomlinson, J., Collins, D. R., Knapp, D., Weinheimer, A. J., Montzka, D. D., Campos, T.
623 and Jimenez, J. L.: Fast airborne aerosol size and chemistry measurements above Mexico City and Central Mexico
624 during the MILAGRO campaign., 2008.

625 Dennison, P. E., Brewer, S. C., Arnold, J. D. and Moritz, M. A.: Large wildfire trends in the western United States,
626 1984–2011, *Geophysical Research Letters*, 41(8), 2928–2933, doi:10.1002/2014gl059576, 2014.

627 Eatough, D. J., Eatough, N. L., Pang, Y., Sizemore, S., Kirchstetter, T. W., Novakov, T. and Hobbs, P. V.: Semivolatile
628 particulate organic material in southern Africa during SAFARI 2000, *J. Geophys. Res. D: Atmos.*, 108(D13)
629 [online] Available from:
630 <https://agupubs.onlinelibrary.wiley.com/doi/abs/10.1029/2002JD002296>%4010.1002/%28ISSN%292169-8996.SAF
631 1, 2003.

632 Evans, J. D. (1996). *Straightforward statistics for the behavioral sciences*. Thomson Brooks/Cole Publishing Co.

633 Ford, B., Val Martin, M., Zelasky, S. E., Fischer, E. V., Anenberg, S. C., Heald, C. L. and Pierce, J. R.: Future Fire Impacts
634 on Smoke Concentrations, Visibility, and Health in the Contiguous United States, *GeoHealth*,
635 doi:10.1029/2018GH000144, 2018.

636 Formenti, P., Elbert, W., Maenhaut, W., Haywood, J., Osborne, S. and Andreae, M. O.: Inorganic and carbonaceous aerosols
637 during the Southern African Regional Science Initiative (SAFARI 2000) experiment: Chemical characteristics,
638 physical properties, and emission data for smoke from African biomass burning, *J. Geophys. Res. D: Atmos.*,
639 108(D13), doi:10.1029/2002JD002408, 2003.

640 Forrister, H., Liu, J., Scheuer, E., Dibb, J., Ziemba, L., Thornhill, K. L., Anderson, B., Diskin, G., Perring, A. E., Schwarz, J.
641 P., Campuzano–Jost, P., Day, D. A., Palm, B. B., Jimenez, J. L., Nenes, A. and Weber, R. J.: Evolution of brown
642 carbon in wildfire plumes, *Geophys. Res. Lett.*, 42(11), 4623–4630, 2015.

643 Gan, R. W., Ford, B., Lassman, W., Pfister, G., Vaidyanathan, A., Fischer, E., Volckens, J., Pierce, J. R. and Magzamen, S.:
644 Comparison of wildfire smoke estimation methods and associations with cardiopulmonary-related hospital
645 admissions, *GeoHealth*, 1(3), 122–136, 2017.

646 Garofalo, L., Pothier, M. A., Levin, E. J. T., Campos, T., Kreidenweis, S. M. and Farmer, D. K.: Emission and Evolution of
647 Submicron Organic Aerosol in Smoke from Wildfires in the Western United States, *ACS Earth and Space*
648 *Chemistry*, acsearthspacechem.9b00125, 2019.

649 Giglio, L., Csiszar, I. and Justice, C. O.: Global distribution and seasonality of active fires as observed with the Terra and
650 Aqua Moderate Resolution Imaging Spectroradiometer (MODIS) sensors, *Journal of Geophysical Research:*
651 *Biogeosciences*, 111(G2) [online] Available from:
652 <https://agupubs.onlinelibrary.wiley.com/doi/abs/10.1029/2005JG000142>, 2006.

653 Giglio, L., Csiszar, I., Restás, Á., Morissette, J. T., Schroeder, W., Morton, D. and Justice, C. O.: Active fire detection and
654 characterization with the advanced spaceborne thermal emission and reflection radiometer (ASTER), *Remote*
655 *Sensing of Environment*, 112(6), 3055–3063, doi:10.1016/j.rse.2008.03.003, 2008.

656 Gilman, J. B., Lerner, B. M., Kuster, W. C., Goldan, P. D., Warneke, C., Veres, P. R., Roberts, J. M., De Gouw, J. A., Burling,
657 I. R. and Yokelson, R. J.: Biomass burning emissions and potential air quality impacts of volatile organic
658 compounds and other trace gases from fuels common in the US, *Atmos. Chem. Phys.*, 15(24), 13915–13938, 2015.

659 Grieshop, A. P., Logue, J. M., Donahue, N. M., and Robinson, A. L.: Laboratory investigation of photochemical oxidation of
660 organic aerosol from wood fires 1: measurement and simulation of organic aerosol evolution, *Atmos. Chem. Phys.*,
661 9, 1263–1277, <https://doi.org/10.5194/acp-9-1263-2009>, 2009.

662 Hatch, L. E., Luo, W., Pankow, J. F., Yokelson, R. J., Stockwell, C. E. and Barsanti, K. C.: Identification and quantification
663 of gaseous organic compounds emitted from biomass burning using two-dimensional gas
664 chromatography-time-of-flight mass spectrometry, *Atmos. Chem. Phys.*, 15(4), 1865–1899, 2015.

665 Hatch, L. E., Yokelson, R. J., Stockwell, C. E., Veres, P. R., Simpson, I. J., Blake, D. R., Orlando, J. J. and Barsanti, K. C.:
666 Multi-instrument comparison and compilation of non-methane organic gas emissions from biomass burning and
667 implications for smoke-derived secondary organic aerosol precursors, *Atmos. Chem. Phys.*, 17, 1471–1489, 2017.

668 Heald, C. L., Kroll, J. H., Jimenez, J. L., Docherty, K. S., DeCarlo, P. F., Aiken, A. C., Chen, Q., Martin, S. T., Farmer, D. K.
669 and Artaxo, P.: A simplified description of the evolution of organic aerosol composition in the atmosphere,
670 *Geophys. Res. Lett.*, 37(8), doi:10.1029/2010GL042737, 2010.

671 Hecobian, A., Liu, Z., Hennigan, C. J., Huey, L. G., Jimenez, J. L., Cubison, M. J., Vay, S., Diskin, G. S., Sachse, G. W.,
672 Wisthaler, A., Mikoviny, T., Weinheimer, A. J., Liao, J., Knapp, D. J., Wennberg, P. O., Urten, A., Crouse, J. D.,
673 Clair, J. S., Wang, Y. and Weber, R. J.: Comparison of chemical characteristics of 495 biomass burning plumes
674 intercepted by the NASA DC-8 aircraft during the ARCTAS/CARB-2008 field campaign, *Atmos. Chem. Phys.*, 11,
675 13325–13337, 2011.

676 Hennigan, C. J., Miracolo, M. A., Engelhart, G. J., May, A. A., Presto, A. A., Lee, T., Sullivan, A. P., McMeeking, G. R.,
677 Coe, H., Wold, C. E., Hao, W. M., Gilman, J. B., Kuster, W. C., De Gouw, J., Schichtel, B. A., Collett, J. L.,
678 Kreidenweis, S. M. and Robinson, A. L.: Chemical and physical transformations of organic aerosol from the
679 photo-oxidation of open biomass burning emissions in an environmental chamber, *Atmos. Chem. Phys.*, 11(15),
680 7669–7686, doi:10.5194/acp-11-7669-2011, 2011.

681 Hobbs, P. V., Sinha, P., Yokelson, R. J., Christian, T. J., Blake, D. R., Gao, S., Kirchstetter, T. W., Novakov, T. and Pilewskie,
682 P.: Evolution of gases and particles from a savanna fire in South Africa, *J. Geophys. Res. D: Atmos.*, 108(D13),
683 doi:10.1029/2002JD002352, 2003.

684 Hodshire, A. L., Akherati, A., Alvarado, M. J., Brown-Steiner, B., Jathar, S. H., Jimenez, J. L., Kreidenweis, S. M.,
685 Lonsdale, C. R., Onasch, T. B., Ortega, A. M. and Pierce, J. R.: Aging Effects on Biomass Burning Aerosol Mass
686 and Composition: A Critical Review of Field and Laboratory Studies, *Environ. Sci. Technol.*, 53(17), 10007–10022,
687 2019a.

688 Hodshire, A. L., Bian, Q., Ramnarine, E., Lonsdale, C. R., Alvarado, M. J., Kreidenweis, S. M., Jathar, S. H. and Pierce, J.
689 R.: More than emissions and chemistry: Fire size, dilution, and background aerosol also greatly influence near-field
690 biomass burning aerosol aging, *J. Geophys. Res. D: Atmos.*, 2018JD029674, 2019b.

691 Huffman, J. A., Docherty, K. S., Aiken, A. C., Cubison, M. J., Ulbrich, I. M., Decarlo, P. F., Sueper, D., Jayne, J. T.,
692 Worsnop, D. R., Ziemann, P. J. and Jimenez, J. L.: Chemically-resolved aerosol volatility measurements from two
693 megacity field studies., 2009.

694 Janhäll, S., Andreae, M. O. and Pöschl, U.: Biomass burning aerosol emissions from vegetation fires: particle number and
695 mass emission factors and size distributions, *Atmos. Chem. Phys. Disc.*, 9(4), 17183–17217, 2009.

696 Jen, C. N., Hatch, L. E., Selimovic, V., Yokelson, R. J., Weber, R., Fernandez, A. E., Kreisberg, N. M., Barsanti, K. C. and
697 Goldstein, A. H.: Speciated and total emission factors of particulate organics from burning western US wildland
698 fuels and their dependence on combustion efficiency, *Atmos. Chem. Phys.*, 19, 1013–1026, 2019.

699 Jimenez, J. L., Canagaratna, M. R., Donahue, N. M., Prevot, a. S. H., Zhang, Q., Kroll, J. H., DeCarlo, P. F., Allan, J. D.,
700 Coe, H., Ng, N. L., Aiken, a. C., Docherty, K. S., Ulbrich, I. M., Grieshop, a. P., Robinson, a. L., Duplissy, J.,
701 Smith, J. D., Wilson, K. R., Lanz, V. a., Hueglin, C., Sun, Y. L., Tian, J., Laaksonen, A., Raatikainen, T., Rautiainen,
702 J., Vaattovaara, P., Ehn, M., Kulmala, M., Tomlinson, J. M., Collins, D. R., Cubison, M. J., Dunlea, E. J., Huffman,
703 J. a., Onasch, T. B., Alfarra, M. R., Williams, P. I., Bower, K., Kondo, Y., Schneider, J., Drewnick, F., Borrmann, S.,
704 Weimer, S., Demerjian, K., Salcedo, D., Cottrell, L., Griffin, R., Takami, A., Miyoshi, T., Hatakeyama, S., Shimonono,
705 A., Sun, J. Y., Zhang, Y. M., Dzepina, K., Kimmel, J. R., Sueper, D., Jayne, J. T., Herndon, S. C., Trimborn, a. M.,
706 Williams, L. R., Wood, E. C., Middlebrook, a. M., Kolb, C. E., Baltensperger, U. and Worsnop, D. R.: Evolution of
707 organic aerosols in the atmosphere, *Science*, 326(5959), 1525–1529, 2009.

708 Jolleys, M. D., Coe, H., McFiggans, G., Capes, G., Allan, J. D., Crosier, J., Williams, P. I., Allen, G., Bower, K. N., Jimenez,
709 J. L., Russell, L. M., Grutter, M. and Baumgardner, D.: Characterizing the aging of biomass burning organic aerosol
710 by use of mixing ratios: A meta-analysis of four regions, *Environmental Science and Technology*, 46(24),
711 13093–13102, 2012.

712 Jolleys, M. D., Coe, H., McFiggans, G., Taylor, J. W., O’Shea, S. J., Le Breton, M., Bauguitte, S. J. B., Moller, S., Di Carlo,
713 P., Aruffo, E., Palmer, P. I., Lee, J. D., Percival, C. J. and Gallagher, M. W.: Properties and evolution of biomass
714 burning organic aerosol from Canadian boreal forest fires, *Atmos. Chem. Phys.*, 15(6), 3077–3095, 2015.

715 Kleinman, L. I., Daum, P. H., Lee, Y. N., Senum, G. I., Springston, S. R., Wang, J., Berkowitz, C., Hubbe, J., Zaveri, R. A.,
716 Brechtel, F. J., Jayne, J., Onasch, T. B. and Worsnop, D.: Aircraft observations of aerosol composition and ageing in
717 New England and Mid-Atlantic States during the summer 2002 New England Air Quality Study field campaign, *J.*
718 *Geophys. Res. Atmos.*, 112(9), 1–18, doi:10.1029/2006JD007786, 2007.

719 Kleinman, L. and Sedlacek, A. J., III: Biomass Burning Observation Project (BBOP) Final Campaign Report, 2016.

720 Kleinman, L. I., Sedlacek, A. J., III, Adachi, K., Buseck, P. R., Collier, S., Dubey, M., K., Hodshire, A. L., Lewis, E.,
721 Onasch, T. B., Pierce, J. R., Schilling, J., Springston, S. R., Wang, J., Zhang, Q., Zhoui, S., Yokelson, R. J.: Rapid
722 Evolution of Aerosol Particles and their Optical Properties Downwind of Wildfires in the Western U.S., submitted
723 to *Atmos. Chem. Phys.*, 2020.

724 Kononov, I. B., Beekmann, M., Golovushkin, N. A. and Andreae, M. O.: Nonlinear behavior of organic aerosol in biomass
725 burning plumes: a microphysical model analysis, *Atmos. Chem. Phys. Disc.*, 1–44, 2019.

726 Koss, A. R., Sekimoto, K., Gilman, J. B., Selimovic, V., Coggon, M. M., Zarzana, K. J., Yuan, B., Lerner, B. M., Brown, S.
727 S., Jimenez, J. L., Krechmer, J., Roberts, J. M., Warneke, C., Yokelson, R. J. and De Gouw, J.: Non-methane
728 organic gas emissions from biomass burning: Identification, quantification, and emission factors from PTR-ToF
729 during the FIREX 2016 laboratory experiment, *Atmos. Chem. Phys.*, 18(5), 3299–3319, 2018.

730 Kroll, J. H. and Seinfeld, J. H.: Chemistry of secondary organic aerosol: Formation and evolution of low-volatility organics
731 in the atmosphere, *Atmos. Environ.*, 42, 3593–3624, 2008.

732 Kulkarni, P. and Wang, J.: New fast integrated mobility spectrometer for real-time measurement of aerosol size
733 distribution—I: Concept and theory, *J. Aerosol Sci.*, 37(10), 1303–1325, 2006.

734 Lee, J. E., Dubey, M. K., Aiken, A. C., Chylek, P., & Carrico, C. M.: Optical and chemical analysis of absorption
735 enhancement by mixed carbonaceous aerosols in the 2019 Woodbury, AZ fire plume, *J. Geophys. Res. Atmos.*, 125,
736 e2020JD032399. <https://doi.org/10.1029/2020JD032399>, 2020.

737 Lee, T., Sullivan, A. P., Mack, L., Jimenez, J. L., Kreidenweis, S. M., Onasch, T. B., Worsnop, D. R., Malm, W., Wold, C. E.,
738 Hao, W. M. and Collett, J. L.: Chemical Smoke Marker Emissions During Flaming and Smoldering Phases of
739 Laboratory Open Burning of Wildland Fuels, *Aerosol Sci. Technol.*, 44(9), i–v, 2010.

740 Lim, C. Y., Hagan, D. H., Coggon, M. M., Koss, A. R., Sekimoto, K., de Gouw, J., Warneke, C., Cappa, C. D., and Kroll, J.
741 H.: Secondary organic aerosol formation from the laboratory oxidation of biomass burning emissions, *920 Atmos.*
742 *Chem. Phys.*, 19, 12797–12809, 10.5194/acp-19-12797-2019, 2019.

743 Liu, X., Zhang, Y., Huey, L. G., Yokelson, R. J., Wang, Y., Jimenez, J. L., Campuzano-Jost, P., Beyersdorf, A. J., Blake, D.
744 R., Choi, Y., St. Clair, J. M., Crouse, J. D., Day, D. A., Diskin, G. S., Ried, A., Hall, S. R., Hanisco, T. F., King, L.
745 E., Meinardi, S., Mikoviny, T., Palm, B. B., Peischl, J., Perring, A. E., Pollack, I. B., Ryerson, T. B., Sachse, G.,
746 Schwarz, J. P., Simpson, I. J., Tanner, D. J., Thornhil, K. L., Ullmann, K., Weber, R. J., Wennberg, P. O., Wisthaler,
747 A., Wolfe, G. M. and Ziemba, L. D.: Agricultural fires in the southeastern U.S. during SEAC4RS: Emissions of
748 trace gases and particles and evolution of ozone, reactive nitrogen, and organic aerosol, *J. Geophys. Res.*, 121(12),
749 7383–7414, 2016.

750 Liu, P.S.K., Deng, R., Smith, K.A., Williams, L.R., Jayne, J.T., Canagaratna, M.R., Moore, K., Onasch, T.B., Worsnop, D.R.,
751 and Deshler, T.: Transmission Efficiency of an Aerodynamic Focusing Lens System: Comparison of Model
752 Calculations and Laboratory Measurements for the Aerodyne Aerosol Mass Spectrometer, *Aerosol Sci. Technol.*,
753 41(8):721–733, 2007Long, C. N., Bucholtz, A., Jonsson, H., Schmid, B., Vogelmann, A. and Wood, J.: A Method
754 of Correcting for Tilt from Horizontal in Downwelling Shortwave Irradiance Measurements on Moving Platforms,
755 *The Open Atmospheric Science Journal*, 4(1), 78–87, doi:10.2174/1874282301004010078, 2010.

756 Massoli, P., Onasch, T. B., Cappa, C. D., Nuamaan, I., Hakala, J., Hayden, K., Li, S., Sueper, D. T., Bates, T. S., Quinn, P. K.,
757 Jayne, J. T., and Worsnop, D. R.: Characterization of black carbon-containing particles from soot particle aerosol

758 mass spectrometer measurements on the R/V *Atlantis* during CalNex 2010. *J. Geophys. Res. Atmos.*, 120, 2575–
759 2593. doi: 10.1002/2014JD022834, 2015.

760 May, A. A., Levin, E. J. T., Hennigan, C. J., Riipinen, I., Lee, T., Collett, J. L., Jimenez, J. L., Kreidenweis, S. M. and
761 Robinson, A. L.: Gas-particle partitioning of primary organic aerosol emissions: 3. Biomass burning, *J. Geophys.*
762 *Res. D: Atmos.*, 118(19), 11327–11338, 2013.

763 May, A. A., Lee, T., McMeeking, G. R., Akagi, S., Sullivan, A. P., Urbanski, S., Yokelson, R. J. and Kreidenweis, S. M.:
764 Observations and analysis of organic aerosol evolution in some prescribed fire smoke plumes, *Atmos. Chem. Phys.*,
765 15(11), 6323–6335, 2015.

766 McClure, C. D., Lim, C. Y., Hagan, D. H., Kroll, J. H., and Cappa, C. D.: Biomass-burning-derived particles from a wide
767 variety of fuels – Part 1: Properties of primary particles, *Atmos. Chem. Phys.*, 20, 1531-1547,
768 <https://doi.org/10.5194/acp-20-1531-2020>, 2020.

769 Middlebrook, A. M., Bahreini, R., Jimenez, J. L. and Canagaratna, M. R.: Evaluation of composition-dependent collection
770 efficiencies for the Aerodyne aerosol mass spectrometer using field data, *Aerosol Sci. Technol.*, 46(3), 258–271,
771 doi:10.1080/02786826.2011.620041, 2012.

772 Morgan, W. T., Allan, J. D., Bauguitte, S., Darbyshire, E., Flynn, M. J., Lee, J., Liu, D., Johnson, B., Haywood, J., Longo, K.
773 M., Artaxo, P. E. and Coe, H.: Transformation and aging of biomass burning carbonaceous aerosol over tropical
774 South America from aircraft in-situ measurements during SAMBBA, *Atmos. Chem. Phys. Discuss.*,
775 doi:10.5194/acp-2019-157, 2019.

776 Moteki, N. and Kondo, Y.: Dependence of Laser-Induced Incandescence on Physical Properties of Black Carbon Aerosols:
777 Measurements and Theoretical Interpretation, *Aerosol Sci. Technol.*, 44(8), 663–675, 2010.

778 Nance, J. D., Hobbs, P. V. and Radkel, L. F.: Airborne Measurements of Gases and Particles From an Alaskan Wildfire, *J.*
779 *Geophys. Res. D: Atmos.*, 98(D8), 873–882, 1993.

780 Noyes, K. J., Kahn, R., Sedlacek, A., Kleinman, L., Limbacher, J. and Li, Z.: Wildfire Smoke Particle Properties and
781 Evolution, from Space-Based Multi-Angle Imaging, *Remote Sensing*, 12(5), 769, doi:10.3390/rs12050769, 2020.

782 O’Dell, K., Ford, B., Fischer, E. V. and Pierce, J. R.: Contribution of Wildland-Fire Smoke to US PM_{2.5} and Its Influence on
783 Recent Trends, *Environmental Science & Technology*, 53(4), 1797–1804, doi:10.1021/acs.est.8b05430, 2019.

784 Olfert, J. S. and Wang, J.: Dynamic Characteristics of a Fast-Response Aerosol Size Spectrometer, *Aerosol Sci. Technol.*,
785 43(2), 97–111, 2009.

786 Onasch, T. B., Trimborn, A., Fortner, E. C., Jayne, J. T., Kok, G. L., Williams, L. R., Davidovits, P. and Worsnop, D. R.:
787 Soot Particle Aerosol Mass Spectrometer: Development, Validation, and Initial Application, *Aerosol Science and*
788 *Technology*, 46(7), 804–817, doi:10.1080/02786826.2012.663948, 2012.

789 Palm, B. B., Peng, Q., Fredrickson, C. D., Lee, B. H., Garofalo, L. A. and Pothier, M. A.: Quantification of organic aerosol
790 and brown carbon evolution in fresh wildfire plumes, , doi:10.1073/pnas.2012218117, 2020.

791 Petters, M. D. and Kreidenweis, S. M.: A single parameter representation of hygroscopic growth and cloud condensation
792 nucleus activity, *Atmos. Chem. Phys.*, 7(8), 1961–1971, 2007.

793 Petters, M. D., Carrico, C. M., Kreidenweis, S. M., Prenni, A. J., DeMott, P. J., Collett, J. L. and Moosmüller, H.: Cloud
794 condensation nucleation activity of biomass burning aerosol, *J. Geophys. Res. D: Atmos.*, 114(22), 22205, 2009.

795 Ramnarine, E., Kodros, J. K., Hodshire, A. L., Lonsdale, C. R., Alvarado, M. J. and Pierce, J. R.: Effects of near-source
796 coagulation of biomass burning aerosols on global predictions of aerosol size distributions and implications for
797 aerosol radiative effects, *Atmos. Chem. Phys.*, 19(9), 6561–6577, 2019.

798 Reid, C. E., Brauer, M., Johnston, F. H., Jerrett, M., Balmes, J. R. and Elliott, C. T.: Critical review of health impacts of
799 wildfire smoke exposure, *Environmental Health Perspectives*, 124(9), 1334–1343, doi:10.1289/ehp.1409277, 2016.

800 Reid, J. S., Hobbs, P. V., Ferek, R. J., Blake, D. R., Martins, J. V., Dunlap, M. R. and Liousse, C.: Physical, chemical, and
801 optical properties of regional hazes dominated by smoke in Brazil, *J. Geophys. Res. D: Atmos.*, 103(D24),
802 32059–32080, 1998.

803 Reid, J. S., Eck, T. F., Christopher, S. A., Koppmann, R., Dubovik, O., Eleuterio, D. P., Holben, B. N., Reid, E. A. and
804 Zhang, J.: A review of biomass burning emissions part III: intensive optical properties of biomass burning particles,
805 *Atmos. Chem. Phys.*, 5, 827–849, 2005.

806 Sakamoto, K. M., Allan, J. D., Coe, H., Taylor, J. W., Duck, T. J. and Pierce, J. R.: Aged boreal biomass-burning aerosol size
807 distributions from BORTAS 2011, *Atmos. Chem. Phys.*, 15(4), 1633–1646, 2015.

808 Sakamoto, K. M., Laing, J. R., Stevens, R. G., Jaffe, D. A. and Pierce, J. R.: The evolution of biomass-burning aerosol size
809 distributions due to coagulation: Dependence on fire and meteorological details and parameterization, *Atmos.*
810 *Chem. Phys.*, 16(12), 7709–7724, 2016.

811 Schwarz, J. P., Gao, R. S., Fahey, D. W., Thomson, D. S., Watts, L. A., Wilson, J. C., Reeves, J. M., Darbeheshti, M.,
812 Baumgardner, D. G., Kok, G. L. and Others: Single-particle measurements of midlatitude black carbon and
813 light-scattering aerosols from the boundary layer to the lower stratosphere, *J. Geophys. Res. D: Atmos.*, 111(D16)
814 [online] Available from: <https://agupubs.onlinelibrary.wiley.com/doi/abs/10.1029/2006JD007076>, 2006.

815 Schwarz, J.P., Spackman, J.R., Gao, R.S., Perring, a. E., Cross, E., Onasch, T.B., Ahern, a., Wrobel, W., Davidovits, P.,
816 Olfert, J., Dubey, M.K., Mazzoleni, C., and Fahey, D.W.:The Detection Efficiency of the Single Particle Soot
817 Photometer, *Aerosol Sci. Technol.*, 44(8):612–628, 2010. Sedlacek, A. J., Iii, Buseck, P. R., Adachi, K., Onasch, T.
818 B., Springston, S. R. and Kleinman, L.: Formation and evolution of Tar Balls from Northwestern US wildfires,
819 *Atmos. Chem. Phys. Discuss.*, (Figure 1), 1–28, 2018.

820 Seinfeld, J. H. and Pandis, S. N.: Atmospheric chemistry and physics: From air pollution to climate change, John Willey &
821 Sons, Inc. , New York, 2006.

822

823 Shrivastava, M., Cappa, C. D., Fan, J., Goldstein, A. H., Guenther, A. B., Jimenez, J. L., Kuang, C., Laskin, A., Martin, S. T.,
824 Ng, N. L. and Others: Recent advances in understanding secondary organic aerosol: Implications for global climate
825 forcing, *Rev. Geophys.*, 55(2), 509–559, 2017.

826 Spracklen, D. V., Mickley, L. J., Logan, J. A., Hudman, R. C., Yevich, R., Flannigan, M. D. and Westerling, A. L.: Impacts
827 of climate change from 2000 to 2050 on wildfire activity and carbonaceous aerosol concentrations in the western
828 United States, *J. Geophys. Res.*, 114(D20), 1418, 2009.

829 Tang, X., Madronich, S., Wallington, T. and Calamari, D.: Changes in tropospheric composition and air quality, *J.*
830 *Photochem. Photobiol. B*, 46(1-3), 83–95, 1998.

831 Tie, X.: Effect of clouds on photolysis and oxidants in the troposphere, *J. Geophys. Res.*, 108(D20), 23,073, 2003.

832 Twomey, S.: Pollution and the planetary albedo, *Atmos. Environ.*, 8(12), 1251–1256, 1974.

833 Vakkari, V., Kerminen, V.-M., Beukes, J. P., Titta, P., van Zyl, P. G., Josipovic, M., Wnter, A. D., Jaars, K., Worsnop, D. R.,
834 Kulmala, M. and Laakso, L.: Rapid changes in biomass burning aerosols by atmospheric oxidation, *Geophys. Res.*
835 *Lett.*, 2644–2651, 2014.

836 Vakkari, V., Beukes, J. P., Dal Maso, M., Aurela, M., Josipovic, M. and van Zyl, P. G.: Major secondary aerosol formation in
837 southern African open biomass burning plumes, *Nat. Geosci.*, 11(8), 580–583, 2018.

838 Volkamer, R., Jimenez, J. L., San Martini, F., Dzepina, K., Zhang, Q., Salcedo, D., Molina, L. T., Worsnop, D. R. and
839 Molina, M. J.: Secondary organic aerosol formation from anthropogenic air pollution: Rapid and higher than
840 expected, *Geophys. Res. Lett.*, 33(17), 4407, 2006.

841 Volkamer, R., Ziemann, P. J. and Molina, M. J.: Secondary Organic Aerosol Formation from Acetylene (C₂H₂): seed effect
842 on SOA yields due to organic photochemistry in the aerosol aqueous phase, *Atmos. Chem. Phys.*, 9(6), 1907–1928,
843 2009.

844 Wang, J., -N. Lee, Y., Daum, P. H., Jayne, J. and Alexander, M. L.: Effects of aerosol organics on cloud condensation nucleus
845 (CCN) concentration and first indirect aerosol effect, *Atmospheric Chemistry and Physics*, 8(21), 6325–6339,
846 doi:10.5194/acp-8-6325-2008, 2008.

847 Willis, M. D., Lee, A. K. Y., Onasch, T. B., Fortner, E. C., Williams, L. R., Lambe, A. T., Worsnop, D. R., and Abbatt, J. P.
848 D.: Collection efficiency of the soot-particle aerosol mass spectrometer (SP-AMS) for internally mixed particulate
849 black carbon, *Atmos. Meas. Tech.*, 7, 4507–4516, <https://doi.org/10.5194/amt-7-4507-2014>, 2014.

850 Yang, M., Blomquist, B. W. and Huebert, B. J.: Constraining the concentration of the hydroxyl radical in a
851 stratocumulus-topped marine boundary layer from sea-to-air eddy covariance flux measurements of
852 dimethylsulfide, *Atmos. Chem. Phys.*, 9(23), 9225–9236, 2009.

853 Yokelson, R. J., Crouse, J. D., DeCarlo, P. F., Karl, T., Urbanski, S., Atlas, E., Campos, T., Shinozuka, Y., Kapustin, V.,
854 Clarke, A. D., Weinheimer, A., Knapp, D. J., Montzka, D. D., Holloway, J., Weibring, P., Flocke, F., Zheng, W.,
855 Toohey, D., Wennberg, P. O., Wiedinmyer, C., Mauldin, L., Fried, A., Richter, D., Walega, J., Jimenez, J. L.,

856 Adachi, K., Buseck, P. R., Hall, S. R. and Shetter, R.: Emissions from biomass burning in the Yucatan, Atmos.
857 Chem. Phys., 9(15), 5785–5812, 2009.

858 Yue, X., Mickley, L. J., Logan, J. A. and Kaplan, J. O.: Ensemble projections of wildfire activity and carbonaceous aerosol
859 concentrations over the western United States in the mid-21st century, Atmospheric Environment, 77, 767–780,
860 doi:10.1016/j.atmosenv.2013.06.003, 2013.

861 Zhou, S., Collier, S., Jaffe, D. A., Briggs, N. L., Hee, J., Sedlacek, A. J., III, Kleinman, L., Onasch, T. B. and Zhang, Q.:
862 Regional influence of wildfires on aerosol chemistry in the western US and insights into atmospheric aging of
863 biomass burning organic aerosol, Atmos. Chem. Phys., 17(3), 2477–2493, 2017.

864

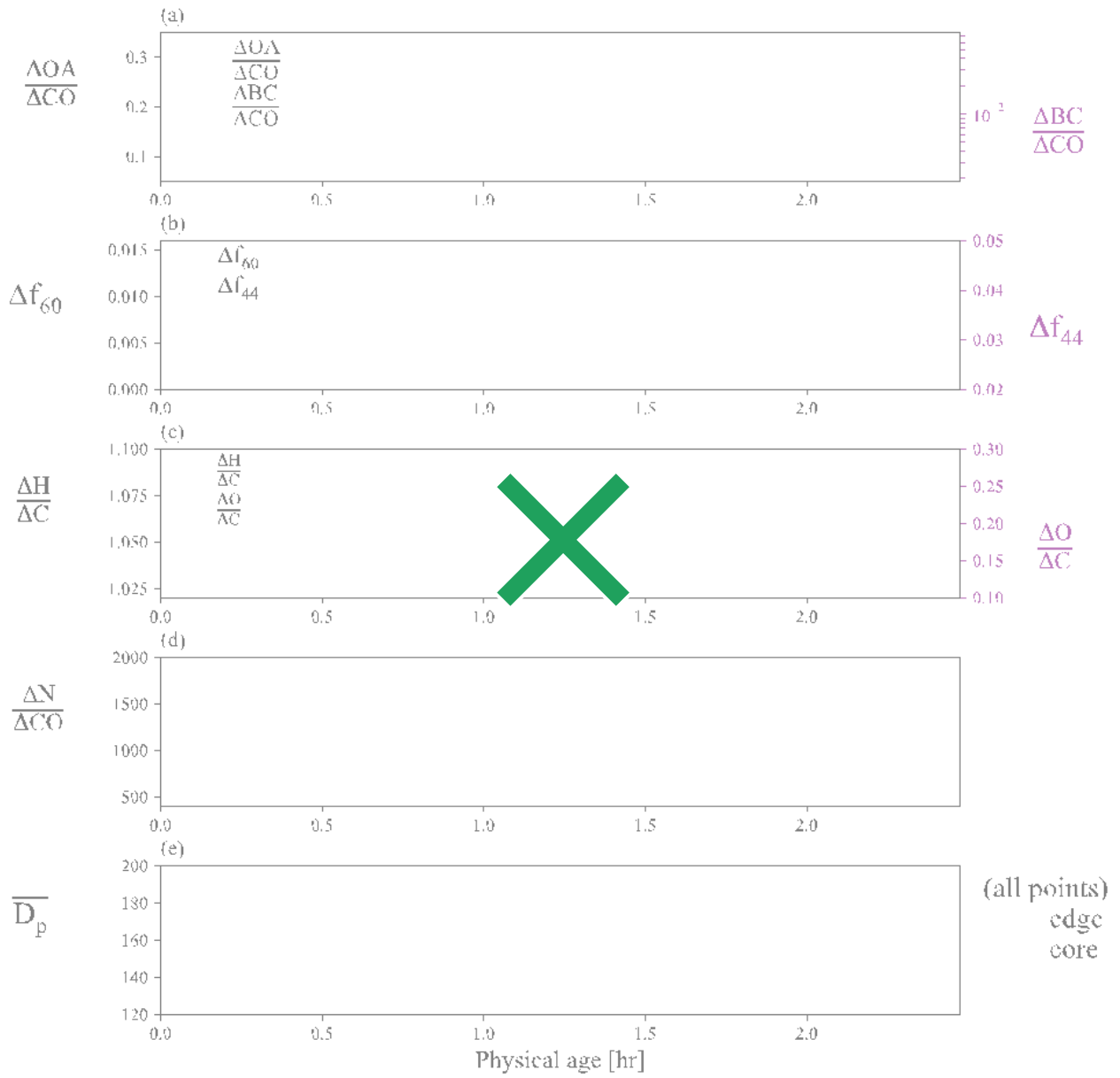
865

866

867

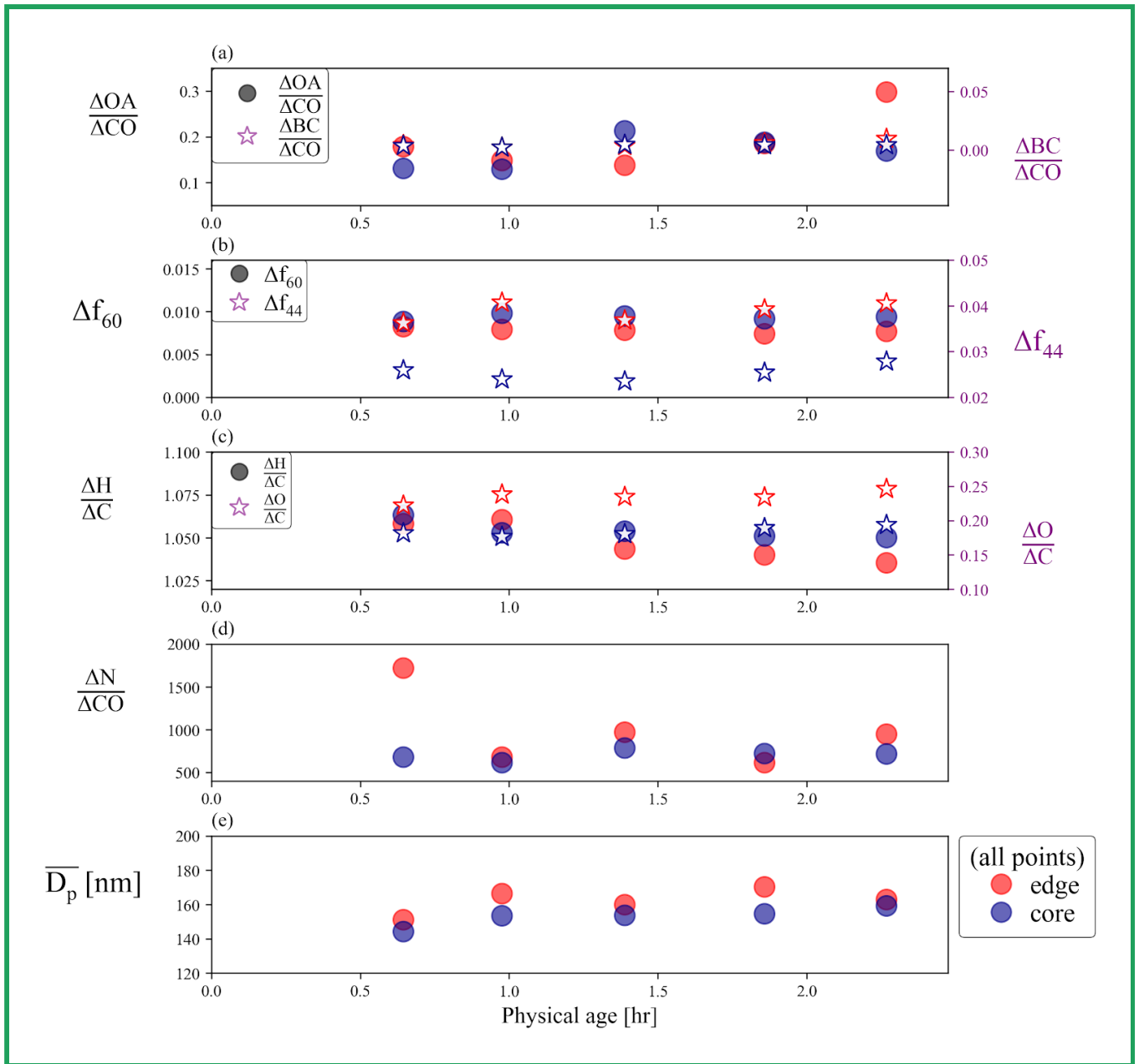
868

869



870

871

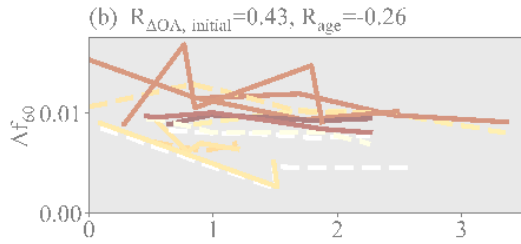
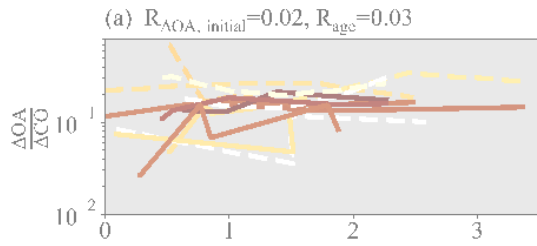


872 **Figure 1: Aerosol properties from the first set of pseudo-Lagrangian transects from the Colockum fire on flight ‘730b’** (a)
 873 $\Delta\text{OA}/\Delta\text{CO}$ (right y-axis) and $\Delta\text{BC}/\Delta\text{CO}$ (left y-axis), (b) Δf_{60} (right y-axis) and Δf_{44} (left y-axis), (c) $\Delta\text{H}/\Delta\text{C}$ (right y-axis) and
 874 $\Delta\text{O}/\Delta\text{C}$ (left y-axis), (d) $\Delta\text{N}/\Delta\text{CO}$, and (e) \overline{D}_p against physical age. For each transect, the data is divided into edge (the lowest
 875 5-15% of ΔCO data; red points) and core (90-100% of ΔCO data; blue points). $\Delta\text{BC}/\Delta\text{CO}$ is shown in log scale to improve clarity.

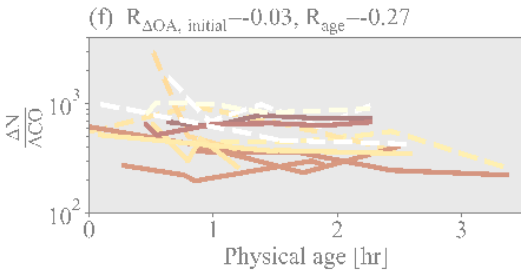
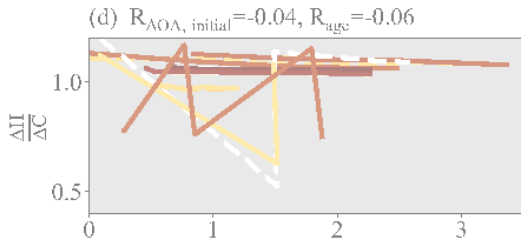
876

877

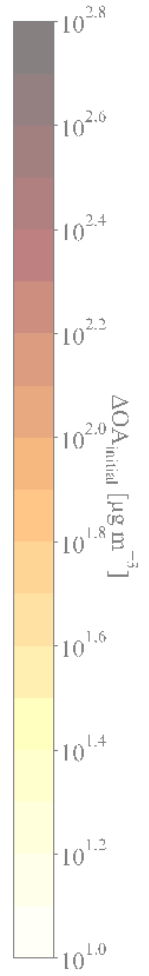
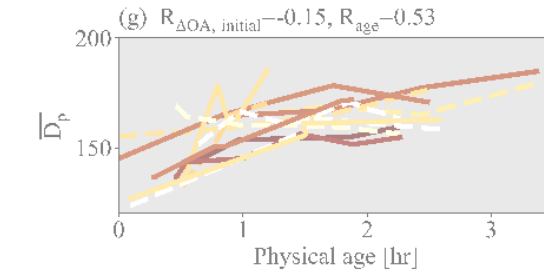
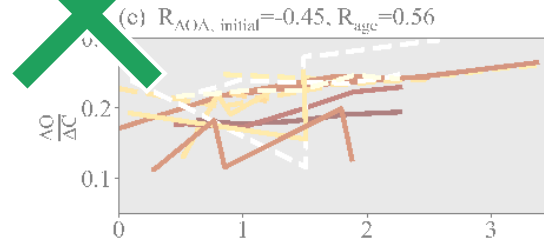
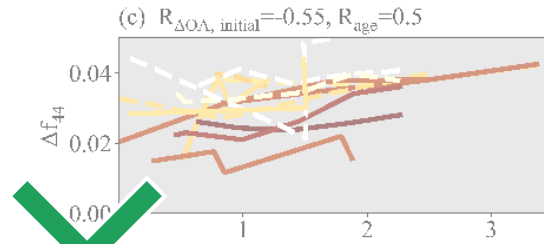
878
879



880

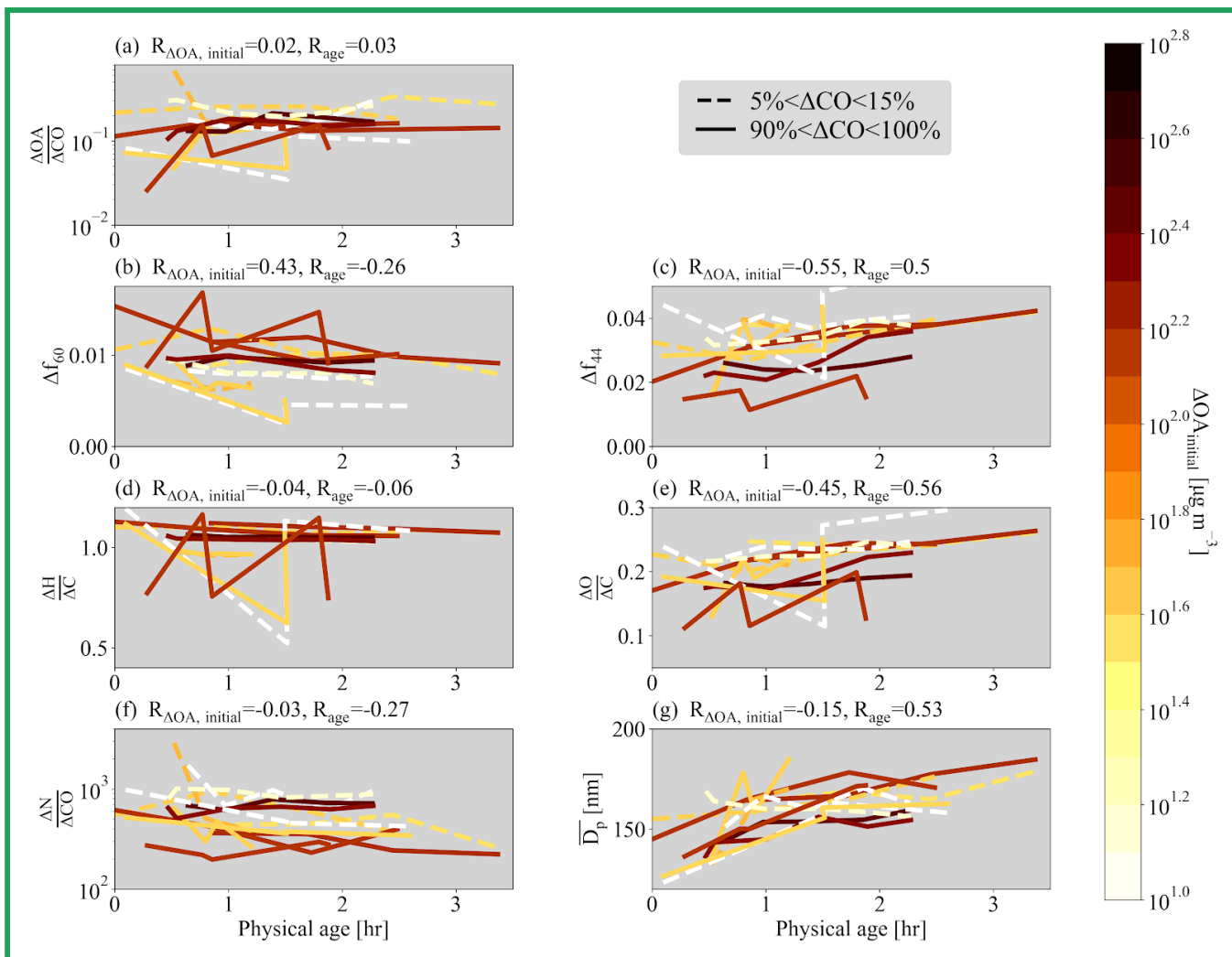


-- 5% < Δ[CO] < 15%
— 90% < Δ[CO] < 100%

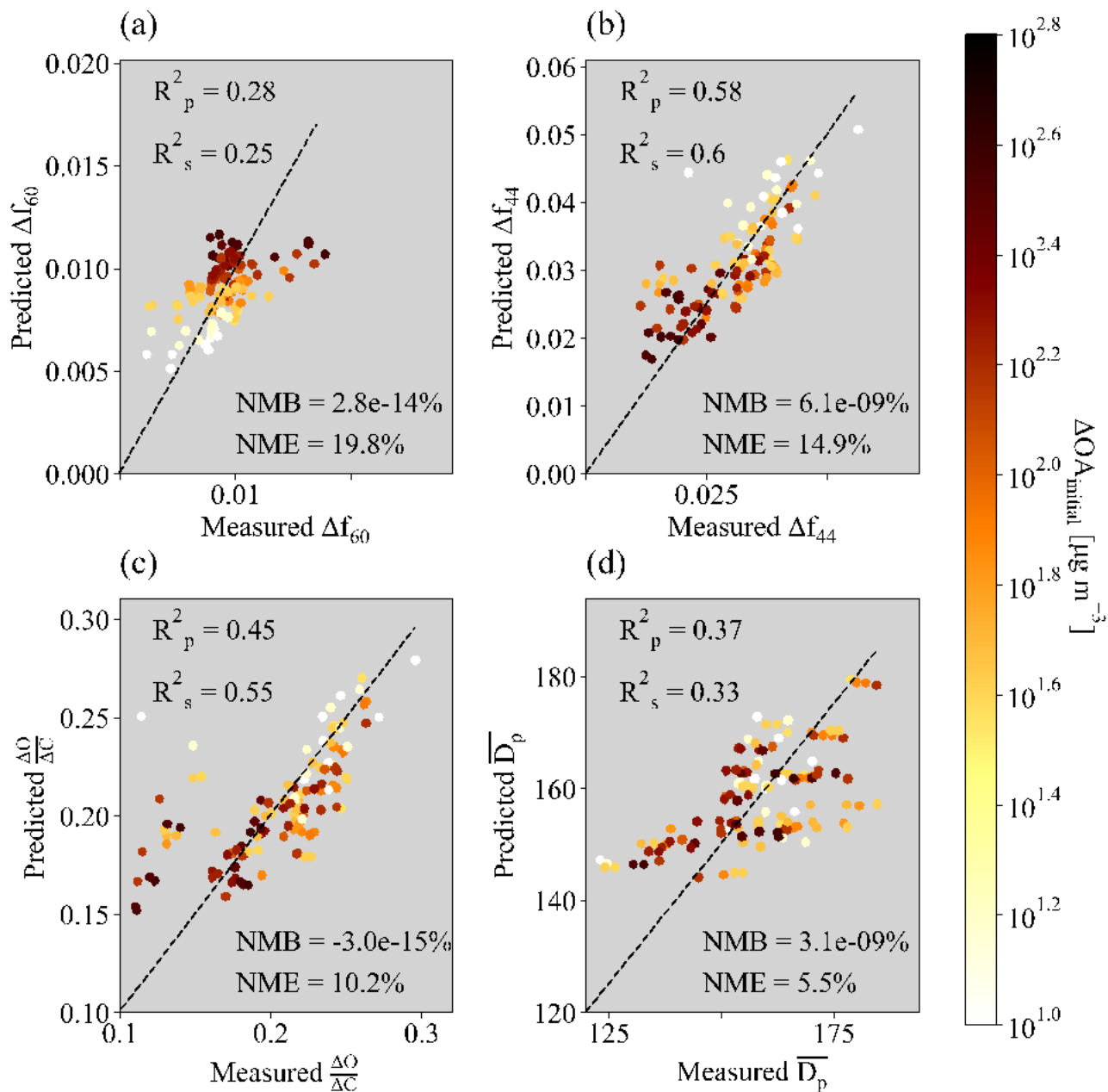


881
882

883



884 **Figure 2. Various normalized parameters as a function of physical age for the 7 sets of pseudo-Lagrangian transects. Separate lines**
 885 **are shown for the edges (lowest 5-15% of ΔCO ; dashed lines) and cores (highest 90-100% of ΔCO ; solid lines). (a) $\Delta OA / \Delta CO$, (b)**
 886 **Δf_{60} , (c) Δf_{44} , (d) $\Delta H / \Delta C$, (e) $\Delta O / \Delta C$, (f) $\Delta N / \Delta CO$, and (g) $\overline{D_p}$ between 40-262 nm against physical age for all flights, colored by**
 887 **$\Delta OA_{\text{initial}}$. Some flights have missing data. Also provided is the Spearman correlation coefficient, R , between each variable and**
 888 **$\Delta OA_{\text{initial}}$ and physical age for each variable. Note that panels (a) and (f), (d), and (g) have a log y-axis.**
 889
 890
 891
 892



893

894

895 **Figure 3.** Measured versus predicted (a) Δf_{60} , (b) Δf_{44} , (c) $\Delta O/\Delta C$, and (d) $\overline{D_p}$ between 40–262 nm. The predicted values are from
 896 the equation $X = a \log_{10}(OA_{initial}) + b$ (Physical age) + c where $X = \Delta f_{60}$, Δf_{44} , $\Delta O/\Delta C$, or $\overline{D_p}$. The values of a , b , and c are provided in
 897 Table S3. The Pearson and Spearman coefficients of determination (R_p^2 and R_s^2 , respectively) are provided in each panel, along
 898 with the normalized mean bias (NMB) and normalized mean error (NME). Note that Fig. 2 provides R values rather than R^2 to

899 provide information upon the trend of the correlation. Included in the fit and figure are points from all four ΔCO regions within
900 the plume (the 5-15%, 15-50%, 50-90%, and 90-100% of ΔCO), all colored by the mean $\Delta OA_{initial}$ of each ΔCO percentile range.
901